Title:
Onset of carbonate biomineralization drove global reorganization of sedimentation and subsidence patterns

Kristin D. Bergmann[1*], Julia Wilcots[1], Tamara Pico[2], Nicholas Boekelheide[1], Noah T. Anderson[1], Marjorie D. Cantine[1,3], Samuel L. Goldberg[1,4], Brenhin Keller[5], Adam B. Jost[1], Athena Eyster[1,6]

[1]Department of Earth, Atmospheric and Planetary Sciences, Massachusetts Institute of Technology, Cambridge, MA 02139

[2]Department of Earth and Planetary Sciences, University of California, Santa Cruz Santa Cruz, CA 95064

[3]now at Department of Geosciences, Goethe-Universität Frankfort, Germany

[4]now at Rosenstiel School of Marine and Atmospheric Science, University of Miami Miami, FL 33149

[5]Department of Earth Sciences, Dartmouth College Hanover, NH 03755

[6]now at Department of Geoscience, University of Wisconsin, Madison Madison, WI 53706

*To whom correspondence should be addressed; E-mail: kdberg@mit.edu.

Carbonate rocks on continental crust are one of Earth's largest reservoirs of CO_2 and yet the controls on their volume through time are poorly understood. Here we quantify temporal changes in preserved continental carbonate rocks over the last billion years in both global and North America-specific datasets

within paleogeographic context. We find the preserved area of continental carbonate rocks increases by $\sim$175$\%$ across the Neoproterozoic–Phanerozoic boundary ca. 539 million years ago, coincident with the rise of macroscopic, multicellular life and the evolutionary innovation of carbonate biomineralization in shallow water reefs. We demonstrate that crustal loading from carbonate sediments on one tropical paleo-continent (North America) contributes to an increase in continent-scale accommodation in the early Phanerozoic, expanding shallow marine environments. We predict this feedback between enhanced carbonate accumulation and subsidence was an important component of the termination of the Great Unconformity. These results are combined into a new conceptual model that links the changes in preserved carbonate rock volumes to the evolutionary innovation of carbonate biomineralization in a range of complex organisms. Our model implies evolutionary controls on the carbonate rock reservoir enhanced CO_2 sequestration at the beginning of the Phanerozoic, with consequences for Earth's carbon cycle, climate and habitability.

One sentence summary: Biomineralization innovations drove increases in the volume of carbonate deposition, global changes in sedimentation patterns, and loading of the crust.

Main Text: The Cambrian Explosion and the Great Ordovician Biodiversification Event in the early Phanerozoic (538.8–$\sim$440 Ma), together are the earliest diversification of animals, including those capable of biomineralization. These evolutionary milestones coincide with striking, enigmatic features of the rock record including: 1) a widespread shift to carbonate deposition in shallow continental seas reaching far into continental interiors following flooding in the early Phanerozoic. This continental flooding terminates what is known as the Great

Unconformity, a time gap between older igneous and sedimentary rocks and Phanerozoic-aged sedimentary rocks (538.8–0 Ma) (*1, 2*), 2) a transition from large magnitude carbon isotope perturbations in carbonate and organic carbon in the Neoproterozoic (1000–538.8 Ma) to more muted δ^{13}C excursions in most of the Phanerozoic(Fig. 1A) (*3*), 3) a secular increase in δ^{18}O values of well-preserved fossils, consistent with long-term global cooling in the early Phanerozoic (Fig. 1B) (*4–8*), and 4) a shift from rare but extreme Snowball Earth glaciations that extended to low-latitudes in the Proterozoic (1000–538.8 Ma) to high latitude glaciations in the Phanerozoic (*9–12*). The co-occurrence of these four enigmatic features of the rock record with the diversification of macroscopic animal life suggest there may be unidentified connections between relative sea-level, carbon cycle dynamics, climate, atmospheric oxygen and Earth's habitability (*9, 10, 13–15*).

Today, carbon and CO_2 are unequally divided between Earth's ocean, atmosphere, terrestrial, and crustal reservoirs, with approximately 80% of near-surface carbon or 6×10^7 GtC stored in carbonate rocks on continental crust (*16*)—changes in the size of this reservoir could have large effects on the global carbon cycle. Projecting observations from the modern carbon cycle backwards in time is a common approach when interpreting the ancient Earth system, yet how far back in time is it reasonable to project modern carbon cycle reservoir sizes and fluxes? Punctuated, sweeping changes to both carbon cycling and storage have been triggered by evolutionary innovations in the biosphere. Early land plant evolution ($\sim$400–350 Ma), enhanced weathering and organic carbon burial on continental crust (*17*). The evolutionary diversification of millimeter-scale planktonic organisms that precipitate $CaCO_3$ skeletons in surface waters far from coasts ($\sim$220–145 Ma) added a new locus of carbonate deposition in deep water environments (*15, 18–20*)(Fig. 1H). In modern oceans, these organisms efficiently sequestering CO_2 and effectively contributing CO_2 to both the mantle and the atmosphere after subduction of

oceanic crust (*15, 20–22*).

The advent of carbonate biomineralization in early complex, macroscopic animals and algae in the early Phanerozoic represents another possible punctuated, large-scale change to a key reservoir in Earth's carbon cycle (Fig. 1G). This evolutionary event drove a shift from abiotic and microbially-mediated carbonates, like stromatolites, in Proterozoic (2500–538.8 Ma) reefs to abundant, thick-shelled, seafloor-dwelling carbonate biomineralizing organisms in Phanerozoic reefs. Despite the fact that this transformation of nearshore reefs occurs within one of Earth's largest carbon reservoirs, carbonate rocks on continental crust, its relative impact as a driver of large-scale carbon-cycle change is less well understood than the rise of land plants or planktonic calcifying organisms. This is, in large part, because skeletons from carbonate biomineralizers do not clearly represent a new carbon sink as carbonate producing shallow-water ecosystems existed throughout the last 3.4 billion years of Earth's history.

Here we explore whether the emergence of biomineralization was a critical driver of early Phanerozoic flooding and changes in the early Phanerozoic carbon cycle and climate. Addressing this question requires a quantitative assessment of the types of sediment being deposited globally through time and their impacts on subsidence and the creation of accommodation, or the space to deposit new sediment. Here we quantify temporal changes in preserved continental carbonate sediments with global, lithology-specific, paleogeographic context over the last billion years. To better constrain the continental carbonate rock reservoir preserved on either side of the Neoproterozoic–Phanerozoic boundary, our approach expands efforts that explored preserved continental sedimentary rock patterns that were temporally limited to the Phanerozoic (*23–28*), or spatially limited (*29*), or lacked lithologic (*30, 31*), or paleogeographic context (*32, 33*). We quantify the contribution from carbonate and siliciclastic sediment loading on accommodation using a North America-specific dataset and consider implications for continen-

tal flooding and the termination of the Great Unconformity. We present a conceptual model that links observed changes in preserved carbonate rock volumes to the advent of carbonate biomineralization. We conclude with predictions for the carbon cycle and climate from our model of a time-varying continental carbonate rock reservoir.

The continental carbonate rock reservoir increased in the early Paleozoic To estimate changes in the size of the continental carbonate rock reservoir through time, we used global and regional geologic maps to tabulate the area of siliciclastic, carbonate, and mixed carbonate-siliciclastic sedimentary rocks through time. Results of this tabulation are explored as area, area/Ma, binned fraction of each sediment type, and binned fraction of all sediment types (Fig. 1,S1,S2,S3,S4). When area is binned by paleolatitude, carbonates and mixed systems invariably tend to form in equatorial regions (Fig. 1C). Despite significant equatorial continental landmasses in the Neoproterozoic, carbonates are not a dominant sediment type until the Cambrian (Cm, 538.8–485.4 Ma, Fig. 1). Neoproterozoic equatorial mixed carbonate-siliciclastic sediment deposits are preserved even when carbonate deposits are not (Fig. 1C, Movie S1). The Cretaceous and early Phanerozoic have the largest area of carbonate rocks, reflecting periods of continental inundation (See probability density functions in Fig. 1C, K and Cm–O, respectively). There is a $\sim$175$\%$ increase in total carbonate area across the Neoproterozoic–Phanerozoic transition (Fig. S1). While the global increase in binned area appears abrupt, it is more likely that there is a gradual increase in carbonate rock area observed across the Cambrian and Ordovician similar to what is observed in the higher resolution North American Macrostrat database. A gradual increase would likely reflect long-lived transgression and relative sea level rise associated with the termination of the Great Unconformity (see Fig. 1G (solid blue line), 2, 3) (*29*). Siliciclastic rocks dominate in mid-latitudes through time and decrease in area by $\sim$15$\%$ across the Neoproterozoic–Phanerozoic transition (Fig. S1).

We also see striking differences in the preserved sedimentary record of each continent (Fig. S3,S4). The increase in carbonate area in the early Phanerozoic is concentrated on four paleo-equatorial landmasses: North America, Siberia, North China, and South China (Fig. 2A, Figs. S3,S4,S5,S6, Movie S1). Conversely, continents at higher paleo-latitudes do not show this increase. These results are based on surface exposures on each continent with differences in mapping resolution. A next step would combine continent scale surface observations with subsurface constraints as has been done in North America (*29*).

Erosion is an undeniable control on the preserved rock record and is commonly invoked to explain temporal changes in the volume of sedimentary rocks, yet predictions from erosion-dominated models do not fit the preserved carbonate and siliciclastic patterns. To assess whether the early Phanerozoic increase in carbonate rocks can be explained solely by erosive processes, we compare preservation patterns in carbonate and siliciclastic rocks, assuming that erosion will have affected both in similar ways. Results are reported as binned proportions defined as the area of a given rock type preserved during an interval of time divided by the total area of that rock type summed across the entire rock record (Figure 1D,E). The fraction of the total carbonate rock area within four time bins makes distinct, stepwise changes while the fraction of the total siliciclastic area within four time bins monotonically increases towards the modern (Fig. 1D,E, bins are 2500–538.8, 538.8–358.9, 358.9–145, 145–0 Ma). The four time bins represent 43%, 3.9% 4.7%, and 3.2% of Earth history, respectively. Another way to assess erosional biases is to consider the proportion of carbonate rocks to all sedimentary rocks at a given point in time. We compared estimates of the proportion of carbonate to all sedimentary rocks from four datasets relevant to the continental rock reservoir (Fig. 1F). These four datasets suggest carbonate rocks increase from $\sim$10–20% of all rock types in the Neoproterozoic to $\sim$30–70% of all rock types in early Phanerozoic rocks, depending on the data source (Fig. 1F).

For comparison, we also calculated the proportion of deep-sea carbonates to all deep-sea sediments since the Jurassic using three available compilations. Even if erosion has removed a Proterozoic continental carbonate rock reservoir that rivaled today's (i.e., during the Grenville Orogeny (*34*), the first Neoproterozoic Snowball Earth glaciation (*2, 35*), or the younger Pan-African and Trans-Antarctic Orogenies (*36*)), our results require that carbonates would have been selectively removed relative to other Proterozoic sediments. Furthermore, Mesoproterozoic and early Neoproterozoic erosive events would still leave more than a hundred million years (650–$\sim$500 Ma) without a large continental carbonate rock reservoir and the growth of the reservoir in the early Phanerozoic would remain consequential for carbon sequestration dynamics.

Geodynamic triggers must also be considered as possible drivers of the observed continental carbonate reservoir signature. Tectonically driven continental emergence can be linked to enhanced weathering of continental crust and increased oceanic alkalinity, favoring carbonate precipitation. Proposed tectonic triggers for emergence or flooding include 1) shifting global tectonothermal stages (e.g. (*37, 38*)), 2) secular cooling of the Earth (e.g. (*39*)), and 3) regional tectonic events, all of which make testable predictions. A tectonothermal shift from hot, thin crust and low orogens spanning from 2000 Ma-800 Ma, to thick, cool crust and modern orogenic styles after 800 Ma is consistent with some datasets (dT/dP and zircon distributions) (*38,40,41*); a Neoproterozoic shift in crustal thickness could impact continental freeboard and weathering (*37*). Alternatively, global models of Earth's secular cooling predict the emergence of continents and coeval acceleration of continental weathering (e.g. (*39, 42, 43*)); recent modeling suggests that large-scale emergence transpired over a 100-300 Ma window, most likely in the Neoproterozoic $\sim$700 Ma (*39*). If current models of either a tectonothermal shift or secular cooling are correct, the timing of tectonic emergence and weathering would predate the

transformation of carbonate deposition by as much as 300 Ma (*38, 39, 41*), although evolving research may add further insights (e.g. (*39, 40*)). In addition to perturbing global weathering, this emergence is predicted to shift the locus of shallow marine carbonate precipitation from intercontinental seas to narrow ribbons of continental shelves (*39*). This prediction is at odds with the dataset we present here—moving carbonate precipitation to narrow continental shelves would likely not increase the area and volume of carbonate sediment in the early Phanerozoic. Buoyant young oceanic crust associated with the breakup of Rodinia has also been suggested as a global driver of early Paleozoic continental flooding, however this fails to match the evidence in our tabulation of equator-dominated flooding and instead would predict latitude-agnostic flooding (*44*). The observed increase in both carbonate and siliciclastic sediment area across all latitudes in the Cretaceous more closely matches the prediction from accommodation increase driven by buoyant young oceanic crust(Fig. 1C).

Regional tectonic events may also act as first-order controls on geochemical cycles and continental emergence or flooding (e.g. (*45*)), yet also poorly explain the temporal, continent-specific, lithologic patterns documented above. Proposed regional tectonic models of global weathering and emergence or flooding include uplift associated with diachronous Neoproterozoic superplume upwelling and rifting (*34, 35, 46–49*), Ediacaran-Cambrian rifting (*50*), or Pan-African (650–500 Ma) and Transantarctic orogenies (615–470 Ma) (*36, 51, 52*). Most of these regional tectonic events significantly predate the Neoproterozoic-Phanerozoic transition (e.g. (*34, 36, 50, 52–54*)). While the Pan-African and Transantarctic orogenies coincide in time, their influences likely dominate on continents not characterized by the most significant early Paleozoic flooding and carbonate deposition. If orogeny-driven weathering was solely responsible for the early Paleozoic carbonate signal, both siliciclastic and carbonate depositional systems should be affected, yet our datasets indicate a dramatic increase in the carbonate rock reservoir

across the early Paleozoic, with no comparable pattern in the siliciclastic reservoir. Regional transformations of continental margins from 'rift to drift' along with thermal subsidence have been suggested as important controls on the early Paleozoic flooding signature in North America (*55*) despite distinct, margin-specific rifting timescales. While any of the above geodynamic paradigms may correctly explain geochemical signals consistent with higher alkalinity by the end of the Proterozoic, a potential precondition for biomineralization (i.e. $^{87}Sr/^{86}Sr$) (*48, 56, 57*), the temporal constraints and and locus of carbonate-dominated deposition in the tropics captured in our datasets in the early Paleozoic are not fully consistent with tectonic predictions.

Carbonate-driven crustal loading feedback contributes to growth of carbonate reservoir

Relative sea-level rise across the Neoproterozoic–Phanerozoic transition inundated many continental interiors after a long period of erosion or non-deposition, terminating the Great Unconformity (*1, 2*). Using a dataset currently only available for North America that includes age, thickness, and areal extent of surface and subsurface rocks (*29*), we first explore the variability of sediment load by creating cross sections of the continent showing both thickness and age of all rock units (i.e., a Wheeler Diagram)(Fig. 2B, Fig. S7) (*29*). The continental margins have thicker deposits of both siliciclastics and carbonates (Fig. 2B, Fig. S7). The continental interior has thinner sedimentary units that are primarily carbonate from ∼500–420 Ma. The sedimentation dataset is used as an input into a gravitationally self-consistent calculation of relative sea level change (or accommodation) across the Neoproterozoic–Phanerozoic boundary(Fig. 3, Figs. S8,S9,S10,S11) (*58*). Given uncertainties in reconstructing lithospheric thickness and mantle rheologies in the Cambrian, we use estimates for a modern North American lithosphere and mantle configuration (*59*).

Our analysis highlights clear lithology-specific differences in the locus and style of sediment loading; accommodation from carbonate loading is continent-wide in the early Phanerozoic

and siliciclastic loading is concentrated in tectonic basins (Fig. 3). From 600–540 Ma, accommodation from carbonate loading (<600 m/10 Myr) is limited to the western and northern North American margins (paleo-northern and eastern respectively). After the Neoproterozoic-Phanerozoic boundary, much of North America experienced 200–1200 m/10 Myr of accommodation from carbonate sediment loading (Fig. 3). Relative sea-level rise from carbonate loading is highest in the Middle to Late Ordovician with ∼1200 meters/10 Myr predicted along the (present-day) western margin (460–450 Ma, Fig. 3). Carbonate-induced subsidence decreases significantly across North America associated with and following the end-Ordovician glaciation (Fig. S10) (*60*). In contrast to the pattern of widespread crustal subsidence associated with carbonate deposition, siliciclastic loading is concentrated within tectonically active basins like the Taconic foreland basin along the modern eastern margin of North America (Figs. S8,S9,S10,S11). Maximum siliciclastic-induced loading is also similar between Ediacaran and early Paleozoic basins (Figs. S8,S9,S10,S11).

Nearshore sediment loading and an increase in accommodation associated with productive, voluminous, tropical carbonate platforms could represent a positive feedback on continent-scale flooding by expanding available shallow marine environments for new carbonate sedimentation. A subsidence feedback from carbonate sedimentation could explain early Paleozoic flooding far into continental interiors and amplify any potential tectonic or glacio-eustatic drivers of relative sea-level rise in the Cambrian and Ordovician (Fig. 1, Cm and O on timescale, respectively) (*2*). From our analysis of global time-constrained lithologic maps (*58*), we observe that the cratons with the largest sediment signal of early Phanerozoic flooding were in the tropics and accumulating carbonate (i.e., North America, and the Siberian, North, and South China cratons)(Figs. S3,S4,S5,S6, Movie S1). Although carbonate sediment area increased substantially on these continents, siliciclastic sediment area and proportion did not increase from the Proterozoic to

Phanerozoic on almost all continents (Figs. S1,S3,S4). This pattern argues against a global cause of extreme sea-level rise and highlights that a defining feature of the Great Unconformity may be synchronous tropical flooding. Tectonic drivers may be fundamentally important for shifting sea water chemistry and nutrient fluxes in the Late Neoproterozoic (*56, 57*), yet the inconsistencies between predictions from existing tectonic frameworks or erosion and our results, including sedimentation patterns and loading dynamics, necessitates a more innovative interpretation of the carbonate system.

Conceptual Model The early Phanerozoic increase in carbonate areal extent and volume in proportion to other sediments combined with our accommodation modeling, lead us to propose a conceptual model to explain carbonate reservoir changes across the Neoproterozoic–Phanerozoic transition. We hypothesize that evolutionary innovations of carbonate biomineralization in organisms in shallow carbonate platforms led to more productive and voluminous carbonate depositional environments with significant progradation (the seaward growth of carbonate platforms). The emergence and expansion of carbonate biomineralization spanned eukaryotic (animal, algal, and protistan) clades and was associated with biochemical, cellular, metabolic, tissual, anatomical, and habitat-scale innovations (*61*). By the latest Proterozoic, biomineralizing organisms evolved mechanisms to overcome kinetic inhibition using membrane-bound pumps that increase the Ca/Mg ratio and pH at the site of calcification, as well as enzymes like carbonic anhydrase, that ultimately boost precipitation rate (*62*). A gradual transformation of the nearshore carbonate factory to one dominated by biomineralizers occurred over the Cambrian Explosion and Great Ordovician Biodiversification event (*63*)(Fig. 4B,C). The growth of the early Paleozoic continental carbonate rock reservoir was a function of both an increase in carbonate production and a positive feedback between efficient biologically-mediated carbonate production, progradation, and subsidence, together enhancing carbon se-

250 questration on continental crust (Fig. 4B,C).

251 By contrast, kinetic and physical inhibitors must have slowed precipitation and ultimately
252 limited production volumes in Proterozoic microbe-dominated reefs. Proterozoic carbonate
253 platforms are primarily dolomite ($CaMg(CO_3)_2$) and much of it likely formed slowly at or near
254 the seafloor((*64*) and references therein). The rock record suggests that without the advantages
255 of biomineralization, Mg^{2+} inhibited carbonate precipitation rates, forcing proto-dolomite or
256 dolomite precipitation in shallow water environments. Trace elements and phosphate have also
257 been invoked as important Proterozoic carbonate kinetic inhibitors at key intervals (*65, 66*).
258 Siliciclastics, like those often found interbedded with Proterozoic shallow water dolomite and
259 deeper water limestone, could have also physically inhibited carbonate precipitation before
260 biomineralizing organisms could construct voluminous reefs far from siliciclastic depocenters
261 (Fig. 4). Less voluminous Proterozoic platforms would have a limited positive feedback on
262 subsidence and regional sea-level trends—despite aggrading to sea-level and having similar
263 platform architectures (*67*).

264 Biomineralizing animals and algae may have increased the range of environments of carbon-
265 ate deposition in the early Paleozoic, but more importantly our results suggest biominerals in
266 combination with a feedback on subsidence increased the total volume of carbonate deposited
267 on continental crust, perhaps taking advantage of a recently created Neoproterozoic alkalinity
268 reservoir (*56, 57*). Building a large early Paleozoic continental carbonate rock reservoir would
269 have ramifications for the long-term carbon cycle and climate.

270 **Predictions for the Carbon Cycle and Climate** In the Precambrian a smaller, more sluggish
271 long-term flux into shallow marine carbonate platforms and a smaller continental carbonate
272 reservoir require other changes in the carbon cycle and weathering to maintain quasi-steady

state over long geologic timescales (*14*). While abiotic processes that add carbonate to the deep sea may have been locally important in the Proterozoic, including water column and seafloor precipitates (*68*), offshore transport of carbonate sediments, and carbonate precipitation associated with serpentinization, we suggest it is unlikely that they would equal the combined sizes of the large continental and deep sea carbonate rock reservoirs we have today (*15, 20, 69–71*). A small deep sea reservoir would imply that the return carbon flux into the mantle during the Precambrian was smaller than today, perhaps resulting in lower volcanic CO_2 outgassing rates despite Earth's warmer interior temperature (Fig. 4A). A deep sea carbonate reservoir smaller than the recent (145–0 Ma) would also not have been able to buffer the carbon cycle during climatic events in the same way it does today (*72*). We estimate inorganic carbon burial flux on continental crust (margins and inland seas) through time (Fig. S2A)despite the imperfect nature of the preserved record (*71*)and compare it to estimates of the recent deep sea burial flux (Fig. S2A). We consider the impact of a smaller carbonate burial flux on inorganic carbon residence time using the modern size of the DIC reservoir over the entire time interval (38973 GtC) or a larger reservoir in the Precambrian and early Paleozoic (101000 GtC) (*73*). Estimated residence times increase to 1-2.5 million years in the Precambrian if one assumes carbonate platforms on continental crust are the dominant carbonate sequestering environment before the evolution of planktonic calcifiying organisms (Fig. S2B). The unique aspects of the Neoproterozoic carbon cycle proposed here (i.e. smaller continental and deep sea carbonate rock reservoirs, sluggish carbon sequestration into microbial and abiotic carbonates, and a gradual increase in alkalinity influx due to tectonic and climatic changes in the Neoproterozoic) may have created different internal dynamics during Neoproterozoic carbon cycle perturbations as evidenced by larger magnitude, longer-lived, carbon isotope excursions in shallow water platform environments (Fig. 1A). In the Phanerozoic both the Cambrian and early Triassic periods are dominated by abiotic and microbial carbonates, high DIC, and high pCO_2(Fig. 1, Cm and Tr on timescale,

respectively). These two time intervals have some of the most extreme carbon isotope perturbations of the Phanerozoic suggesting similar internal feedbacks as the Neoproterozoic (Fig. 1A).

Organic carbon burial, another critical sink of Earth's carbon cycle, could increase alongside carbonate burial in the early Paleozoic (f_{org}) maintaining long-term carbon isotopic compositions (*74*). Multiple models have considered a larger Neoproterozoic dissolved organic carbon pool (*75, 76*). If carbonate loading flooded tropical continents, organic carbon could have been sequestered along with carbonate rocks. This is consistent with evidence that organic carbon burial increased in the sedimentary rocks overlying the Great Unconformity (*77*). By aiding in organic carbon burial, carbonate biomineralization would play a role in increasing atmospheric O_2.

Under the model proposed here (Fig. 4), CO_2 sequestration into voluminous continental carbonates during the early Phanerozoic would shrink the size of the ocean [DIC] reservoir and ultimately atmosphere CO_2, driving cooling. Long-term cooling is consistent with the interpretation that temperature is the primary control on the observed $\delta^{18}O$ increase in well-preserved Paleozoic fossils (*5–8*), and is supported by carbonate clumped isotope temperatures across the early Phanerozoic (*4*)(Fig. 1B). From independent constraints, pCO_2 is also predicted to fall over this time interval (*78*). Elevated temperatures in the Cambrian and early Ordovician, in combination with low dissolved oxygen (*79*), may have stressed early animals; our model of expanding carbonate platforms, ultimately lowering DIC and CO_2, and reducing temperature provides an avenue for relieving the thermal stress these organisms felt (*79*)(Fig. 1, Cm and O on timescale, respectively). Coupled with enhanced weathering in the Neoproterozoic (*47, 48, 56*) and middle to late Ordovician tectonic changes (*10, 80–82*), a biomineralization-driven growth in the carbonate continental rock reservoir could have ultimately helped to cool the

planet leading into the end-Ordovician glaciation by reducing the size of the DIC reservoir.

Conclusions Evolutionary-led changes to the carbon cycle are fundamental to our interpretations of Earth's past climate and environments and to our understanding of the co-evolution of life and our planet. We present evidence that early Phanerozoic shallow water carbonate reefs were voluminous and drove crustal loading and accommodation increase in the tropics, ending the Great Unconformity. Our results underscore an interplay between biomineralization and geodynamics, where efficient carbonate precipitation is actively driving basin development in regions with low relief. This biomineralization-driven change, in addition to others including the evolution of planktonic biomineralization, have the power to influence not just the surface on Earth but also its interior, requiring non-uniformitarian interpretations of carbon cycle reservoirs and fluxes, including volcanic outgassing.

References and Notes

1. S. E. Peters, R. R. Gaines, Formation of the 'Great Unconformity' as a trigger for the Cambrian explosion. *Nature* **484**, 363–6 (2012).

2. C. Brenhin Keller, J. M. Husson, R. N. Mitchell, W. F. Bottke, T. M. Gernon, P. Boehnke, E. A. Bell, N. L. Swanson-Hysell, S. E. Peters, Neoproterozoic glacial origin of the Great Unconformity. *Proc. Natl. Acad. Sci. U. S. A.* **116**, 1136–1145 (2019).

3. M. R. Saltzman, E. Thomas, Carbon Isotope Stratigraphy. *Geol. Time Scale 2012* **1-2**, 207–232 (2012).

4. K. Bergmann, S. Finnegan, R. Creel, J. Eiler, N. Hughes, L. Popov, W. Fischer, A paired apatite and calcite clumped isotope thermometry approach to estimating Cambro-Ordovician seawater temperatures and isotopic composition. *Geochim. Cosmochim. Acta* **224** (2018).

5. J. A. Trotter, I. S. Williams, C. R. Barnes, C. Lécuyer, R. S. Nicoll, Did cooling oceans trigger Ordovician biodiversification? Evidence from conodont thermometry. *Science* **321**, 550–554 (2008).

6. S. L. Goldberg, T. M. Present, S. Finnegan, K. D. Bergmann, A highresolution record of early Paleozoic climate. *Proceedings of the National Academy of Sciences* **118** (2021).

7. J. Veizer, P. Bruckschen, F. Pawellek, A. Diener, O. G. Podlaha, G. A. F. Carden, T. Jasper, C. Korte, H. Strauss, K. Azmy, D. Ala, Oxygen isotope evolution of Phanerozoic seawater. *Palaeogeogr. Palaeoclimatol. Palaeoecol.* **132**, 159–172 (1997).

8. E. Grossman, M. Joachimski, Oxygen isotope stratigraphy. *Geologic Time Scale 2020* (Elsevier, 2020), pp. 279–307.

9. F. A. Macdonald, R. Wordsworth, Initiation of Snowball Earth with volcanic sulfur aerosol emissions. *Geophys. Res. Lett.* **44**, 1938–1946 (2017).

10. F. A. Macdonald, N. L. Swanson-Hysell, Y. Park, L. Lisiecki, O. Jagoutz, Arc-continent collisions in the tropics set Earth's climate state. *Science (80-.).* **364**, 181–184 (2019).

11. P. F. Hoffman, D. S. Abbot, Y. Ashkenazy, D. I. Benn, J. J. Brocks, P. A. Cohen, G. M. Cox, J. R. Creveling, Y. Donnadieu, D. H. Erwin, I. J. Fairchild, D. Ferreira, J. C. Goodman, G. P. Halverson, M. F. Jansen, G. Le Hir, G. D. Love, F. A. Macdonald, A. C. Maloof, C. A. Partin, G. Ramstein, B. E. Rose, C. V. Rose, P. M. Sadler, E. Tziperman, A. Voigt, S. G. Warren, Snowball Earth climate dynamics and Cryogenian geology-geobiology. *Sci. Adv.* **3** (2017).

12. P. F. Hoffman, The Great Oxidation Event and a Siderian Snowball Earth: MIF based correlation of Paleoproterozoic glaciations. *Chem. Geol.* (2013).

13. J. C. Walker, P. B. Hays, J. F. Kasting, A negative feedback mechanism for the long-term stabilization of Earth's surface temperature. *J. Geophys. Res.* **86**, 9776–9782 (1981).

14. T. T. Isson, N. J. Planavsky, Reverse weathering as a long-term stabilizer of marine pH and planetary climate. *Nature* **560**, 471–475 (2018).

15. A. Ridgwell, R. E. Zeebe, The role of the global carbonate cycle in the regulation and evolution of the Earth system. *Earth Planet. Sci. Lett.* **234**, 299–315 (2005).

16. T. T. Isson, N. J. Planavsky, L. Coogan, E. Stewart, J. Ague, E. Bolton, S. Zhang, N. McKenzie, L. Kump, Evolution of the global carbon cycle and climate regulation on earth. *Global Biogeochemical Cycles* **34**, e2018GB006061 (2020).

17. T. W. Dahl, S. K. Arens, The impacts of land plant evolution on Earth's climate and oxygenation state–An interdisciplinary review. *Chemical Geology* **547**, 119665 (2020).

18. A. J. Fraass, D. C. Kelly, S. E. Peters, Macroevolutionary History of the Planktic Foraminifera. *Annu. Rev. Earth Planet. Sci.* **43**, 139–166 (2015).

19. P. R. Bown, J. A. Lees, J. R. Young, Calcareous nannoplankton evolution and diversity through time. *Coccolithophores* (Springer, 2004), pp. 481–508.

20. J. M. Edmond, Y. Huh, Non-steady state carbonate recycling and implications for the evolution of atmospheric pCO_2. *Earth Planet. Sci. Lett.* **216**, 125–139 (2003).

21. R. S. Arvidson, F. T. Mackenzie, R. A. Berner, F. T. Mackenzie, R. A. Berner, The Sensitivity of the Phanerozoic Inorganic Carbon System to the Onset of Pelagic Sedimentation. *Aquat Geochem* **20**, 343–362 (2014).

22. B. H. Wilkinson, Biomineralization, paleoceanography, and the evolution of calcareous marine organisms. *Geology* **7**, 524 (1979).

23. R. S. Arvidson, F. T. Mackenzie, M. Guidry, Magic: A phanerozoic model for the geochemical cycling of major rock-forming components. *American Journal of Science* **306**, 135–190 (2006).

24. R. A. Berner, F. T. Mackenzie, Burial and Preservation of Carbonate Rocks Over Phanerozoic Time. *Aquat. Geochemistry* **17**, 727–733 (2011).

25. F. T. Mackenzie, J. W. Morse, Sedimentary carbonates through Phanerozoic time. *Geochim. Cosmochim. Acta* **56**, 3281–3295 (1992).

26. L. J. Walker, B. H. Wilkinson, L. C. Ivany, Continental Drift and Phanerozoic Carbonate Accumulation in Shallow-Shelf and Deep-Marine Settings. *J. Geol.* **110**, 75–87 (2002).

27. B. H. Wilkinson, T. J. Algeo, Sedimentary carbonate record of calciummagnesium cycling. *Am. J. Sci.* **289**, 1158–1194 (1989).

28. B. H. Wilkinson, B. N. Opdyke, T. J. Algeo, Time partitioning in cratonic carbonate rocks. *Geology* **19**, 1093–1096 (1991).

29. S. E. Peters, J. M. Husson, J. Czaplewski, Macrostrat: a platform for geological data integration and deep-time earth crust research. *Geochemistry, Geophysics, Geosystems* **19**, 1393–1409 (2018).

30. B. H. Wilkinson, B. J. McElroy, S. E. Kesler, S. E. Peters, E. D. Rothman, Global geologic maps are tectonic speedometers - Rates of rock cycling from area-age frequencies. *Bull. Geol. Soc. Am.* **121**, 760–779 (2009).

31. S. E. Peters, J. M. Husson, Sediment cycling on continental and oceanic crust. *Geology* **45**, 323–326 (2017).

32. A. B. Ronov, V. E. Khain, A. N. Balukhovsky, K. B. Seslavinsky, Quantitative analysis of Phanerozoic sedimentation. *Sediment. Geol.* **25**, 311–325 (1980).

33. W. W. Hay, Carbonate sedimentation through the late precambrian and phanerozoic. *Zentralblatt für Geologie und Paläontologie/Teil 1* **1998**, 435–445 (1999).

34. R. M. Flowers, F. A. Macdonald, C. S. Siddoway, R. Havranek, Diachronous development of great unconformities before neoproterozoic snowball earth. *Proceedings of the National Academy of Sciences* **117**, 10172–10180 (2020).

35. M. DeLucia, W. R. Guenthner, S. Marshak, S. Thomson, A. Ault, Thermochronology links denudation of the great unconformity surface to the supercontinent cycle and snowball earth. *Geology* **46**, 167–170 (2018).

420 36. R. J. Squire, I. H. Campbell, C. M. Allen, C. J. Wilson, Did the Transgondwanan Super-
421 mountain trigger the explosive radiation of animals on Earth? *Earth Planet. Sci. Lett.* **250**,
422 116–133 (2006).

423 37. E. Moores, Neoproterozoic oceanic crustal thinning, emergence of continents, and origin
424 of the phanerozoic ecosystem: A model. *Geology* **21**, 5–8 (1993).

425 38. C. J. Spencer, R. N. Mitchell, M. Brown, Enigmatic mid-proterozoic orogens: Hot, thin,
426 and low. *Geophysical Research Letters* **48**, e2021GL093312 (2021).

427 39. C.-T. A. Lee, J. Caves, H. Jiang, W. Cao, A. Lenardic, N. R. McKenzie, O. Shorttle, Q.-z.
428 Yin, B. Dyer, Deep mantle roots and continental emergence: Implications for whole-earth
429 elemental cycling, long-term climate, and the cambrian explosion. *International Geology*
430 *Review* **60**, 431–448 (2018).

431 40. M. Brown, C. Kirkland, T. Johnson, Evolution of geodynamics since the archean: Signif-
432 icant change at the dawn of the phanerozoic. *Geology* **48**, 488–492 (2020).

433 41. C. J. Spencer, Continuous continental growth as constrained by the sedimentary record.
434 *American Journal of Science* **320**, 373–401 (2020).

435 42. N. Vlaar, Continental emergence and growth on a cooling earth. *Tectonophysics* **322**,
436 191–202 (2000).

437 43. N. Flament, N. Coltice, P. F. Rey, A case for late-Archaean continental emergence from
438 thermal evolution models and hypsometry. *Earth Planet. Sci. Lett.* **275**, 326–336 (2008).

439 44. G. C. Bond, P. A. Nickeson, M. A. Kominz, Breakup of a supercontinent between 625 Ma
440 and 555 Ma: new evidence and implications for continental histories. *Earth Planet. Sci.*
441 *Lett.* **70**, 325–345 (1984).

45. K. Sundell, F. Macdonald, The tectonic context of hafnium isotopes in zircon. *Earth and Planetary Science Letters* **584**, 117426 (2022).

46. F. Horton, Did phosphorus derived from the weathering of large igneous provinces fertilize the neoproterozoic ocean? *Geochemistry, Geophysics, Geosystems* **16**, 1723–1738 (2015).

47. Y. Goddéris, Y. Donnadieu, A. Nédélec, B. Dupré, C. Dessert, A. Grard, G. Ramstein, L. M. François, The Sturtian 'snowball' glaciation: Fire and ice. *Earth Planet. Sci. Lett.* **211**, 1–12 (2003).

48. G. M. Cox, G. P. Halverson, R. K. Stevenson, M. Vokaty, A. Poirier, M. Kunzmann, Z. X. Li, S. W. Denyszyn, J. V. Strauss, F. A. Macdonald, Continental flood basalt weathering as a trigger for Neoproterozoic Snowball Earth. *Earth Planet. Sci. Lett.* **446**, 89–99 (2016).

49. Y. Goddéris, Y. Donnadieu, S. Carretier, M. Aretz, G. Dera, M. MacOuin, V. Regard, Onset and ending of the late Palaeozoic ice age triggered by tectonically paced rock weathering. *Nat. Geosci.* **10**, 382–386 (2017).

50. B. Robert, M. Domeier, J. Jakob, On the origins of the Iapetus ocean. *Earth-Science Reviews* **221**, 103791 (2021).

51. Z. Zhu, I. H. Campbell, C. M. Allen, J. J. Brocks, B. Chen, The temporal distribution of earth's supermountains and their potential link to the rise of atmospheric oxygen and biological evolution. *Earth and Planetary Science Letters* **580**, 117391 (2022).

52. J. G. Meert, B. S. Lieberman, The Neoproterozoic assembly of Gondwana and its relationship to the Ediacaran-Cambrian radiation. *Gondwana Res.* **14**, 5–21 (2008).

53. D. C. Bradley, Passive margins through earth history. *Earth-Science Rev.* **91**, 1–26 (2008).

54. D. C. Bradley, Secular trends in the geologic record and the supercontinent cycle (2011).

55. G. C. Bond, M. A. Kominz, M. S. Steckler, J. P. Grotzinger, Role of Thermal Subsidence, Flexure, and Eustasy in the Evolution of Early Paleozoic Passive-Margin Carbonate Platforms (1989).

56. S. T. Brennan, T. K. Lowenstein, J. Horita, Seawater chemistry and the advent of biocalcification. *Geology* **321**, 473–476 (2004).

57. Y. Petrychenko, T. M. Peryt, E. I. Chechel, Early cambrian seawater chemistry from fluid inclusions in halite from siberian evaporites. *Chemical Geology* **219**, 149–161 (2005).

58. Materials and methods are available as supplementary materials at the science website .

59. N. Zhang, S. Zhong, W. Leng, Z.-X. Li, A model for the evolution of the earth's mantle structure since the early paleozoic. *Journal of Geophysical Research: Solid Earth* **115** (2010).

60. S. Finnegan, N. a. Heim, S. E. Peters, W. W. Fischer, Climate change and the selective signature of the Late Ordovician mass extinction. *Proc. Natl. Acad. Sci.* **109**, 6829–6834 (2012).

61. P. U. Gilbert, K. D. Bergmann, N. Boekelheide, S. Tambutté, T. Mass, F. Marin, J. F. Adkins, J. Erez, B. Gilbert, V. Knutson, M. Cantine, J. O. Hernández, A. H. Knoll, Biomineralization: Integrating mechanism and evolutionary history. *Science Advances* **8**, eabl9653 (2022).

62. T. Mass, A. J. Giuffre, C.-Y. Sun, C. A. Stifler, M. J. Frazier, M. Neder, N. Tamura, C. V. Stan, M. A. Marcus, P. U. P. A. Gilbert, Amorphous calcium carbonate particles form coral skeletons. *Proc. Natl. Acad. Sci. U. S. A.* **114**, E7670–E7678 (2017).

485 63. S. B. Pruss, S. Finnegan, W. W. Fischer, A. H. Knoll, Carbonates in skeleton-poor seas:
486 New insights from Cambrian and Ordovician strata of Laurentia. *Palaios* **25**, 73–84
487 (2010).

488 64. M. D. Cantine, A. H. Knoll, K. D. Bergmann, Carbonates before skeletons: A database
489 approach. *Earth-Science Reviews* **201**, 103065 (2020).

490 65. D. Y. Sumner, J. P. Grotzinger, Were kinetics of Archean calcium carbonate precipitation
491 related to oxygen concentration? *Geology* **24**, 119–122 (1996).

492 66. S. Roest-Ellis, J. V. Strauss, N. J. Tosca, Experimental constraints on nonskeletal CaCO3
493 precipitation from Proterozoic seawater. *Geology* **49**, 561–565 (2021).

494 67. J. P. Grotzinger, Facies and evolution of Precambrian carbonate depositional systems:
495 emergence of the modern platform archetype. *Control. carbonate Platf. basin Dev.* pp.
496 71–106 (1989).

497 68. J. A. Higgins, W. W. Fischer, D. P. Schrag, Oxygenation of the ocean and sediments:
498 Consequences for the seafloor carbonate factory. *Earth Planet. Sci. Lett.* **284**, 25–33
499 (2009).

500 69. H. Pälike, *et al.*, A Cenozoic record of the equatorial Pacific carbonate compensation
501 depth. *Nature* **488**, 609–614 (2012).

502 70. A. Paytan, E. M. Griffith, A. Eisenhauer, M. P. Hain, K. Wallmann, A. Ridgwell, A 35-
503 million-year record of seawater stable sr isotopes reveals a fluctuating global carbon cycle.
504 *Science* **371**, 1346–1350 (2021).

505 71. W. W. Hay, Carbonate fluxes and calcareous nannoplankton, *Tech. rep.* (2004).

506 72. A. J. Ridgwell, Carbonate Deposition, Climate Stability, and Neoproterozoic Ice Ages.
507 *Science (80-.).* **302**, 859–862 (2003).

508 73. D. E. Penman, A. D. Rooney, Coupled carbon and silica cycle perturbations during the
509 marinoan snowball earth deglaciation. *Geology* **47**, 317–320 (2019).

510 74. J. M. Hayes, H. Strauss, A. J. Kaufman, The abundance of marine organic matter and
511 isotopic fractionation in the global biogeochemical cycle of carbon during the past 800
512 Ma. *Chem. Geol.* **161**, 103–125 (1999).

513 75. D. H. Rothman, J. M. Hayes, R. E. Summons, Dynamics of the Neoproterozoic carbon
514 cycle. *Proc. Natl. Acad. Sci. USA* **100**, 8124–8129 (2003).

515 76. E. Tziperman, I. Halevy, D. T. Johnston, A. H. Knoll, D. P. Schrag, Biologically induced
516 initiation of Neoproterozoic snowball-Earth events. *Proc. Natl. Acad. Sci. U. S. A.* **108**,
517 15091–6 (2011).

518 77. J. M. Husson, S. E. Peters, Atmospheric oxygenation driven by unsteady growth of the
519 continental sedimentary reservoir. *Earth Planet. Sci. Lett.* **460**, 68–75 (2017).

520 78. D. L. Royer, R. A. Berner, I. P. Montañez, N. J. Tabor, D. J. Beerling, CO_2 as a primary
521 driver of Phanerozoic climate. *GSA Today* **14**, 4 (2004).

522 79. R. G. Stockey, A. Pohl, A. Ridgwell, S. Finnegan, E. A. Sperling, Decreasing Phanero-
523 zoic extinction intensity as a consequence of Earth surface oxygenation and metazoan
524 ecophysiology. *Proceedings of the National Academy of Sciences* **118** (2021).

525 80. O. Jagoutz, F. A. Macdonald, L. Royden, Low-latitude arc-continent collision as a driver
526 for global cooling. *Proc. Natl. Acad. Sci. U. S. A.* **113**, 4935–4940 (2016).

81. S. M. Bergström, W. D. Huff, M. R. Saltzman, D. R. Kolata, S. A. Leslie, The Greatest Volcanic Ash Falls in the Phanerozoic: Trans-Atlantic Relations of the Ordovician Millbrig and Kinnekulle K-Bentonites. *Sediment. Rec.* **2**, 4–8 (2004).

82. S. A. Young, M. R. Saltzman, K. A. Foland, J. S. Linder, L. R. Kump, A major drop in seawater 87Sr/86Sr during the Middle Ordovician (Darriwilian): Links to volcanism and climate? *Geology* **37**, 951–954 (2009).

83. Y. Park, N. L. Swanson-Hysell, S. A. MacLennan, A. C. Maloof, M. Gebreslassie, M. M. Tremblay, B. Schoene, M. Alene, E. S. Anttila, T. Tesema, B. Haileab, The lead-up to the Sturtian Snowball Earth: Neoproterozoic chemostratigraphy time-calibrated by the Tambien Group of Ethiopia. *GSA Bull.* **132**, 1119–1149 (2020).

84. v. d. S. B. F. J. M. C. A. C. G. Bachan, Aviv, J. L. Payne, Carbon cycle dynamics following the end-Triassic mass extinction: Constraints from paired $\delta^{13}\mathrm{C}_carb$ and $\delta^{13}\mathrm{C}_org$ records. *Geochemistry, Geophysics, Geosystems* **13** (2012).

85. A. C. Maloof, S. M. Porter, J. L. Moore, F. O. Dudas, S. A. Bowring, J. A. Higgins, D. A. Fike, M. P. Eddy, The earliest Cambrian record of animals and ocean geochemical change. *Geol. Soc. Am. Bull.* **122**, 1731–1774 (2010).

86. C. Yang, A. D. Rooney, D. J. Condon, X.-H. Li, D. V. Grazhdankin, F. T. Bowyer, C. Hu, F. A. Macdonald, M. Zhu, The tempo of Ediacaran evolution. *Science advances* **7**, eabi9643 (2021).

87. S.-T. Kim, J. R. O'Neil, Equilibrium and nonequilibrium oxygen isotope effects in synthetic carbonates. *Geochim. Cosmochim. Acta* **61**, 3461–3475 (1997).

548 88. J. Hartmann, N. Moosdorf, The new global lithological map database GLiM: A repre-
549 sentation of rock properties at the Earth surface. *Geochemistry, Geophys. Geosystems* **13**
550 (2012).

551 89. The data were downloaded from the EarthChem Portal on February 7, 2017, using the
552 following parameters: rock classification = sedimentary, http://portal.earthchem.org.

553 90. S. E. Peters, M. McClennen, The Paleobiology Database application programming inter-
554 face. *Paleobiology* **42**, 1–7 (2015).

555 91. F. M. Persits, T. S. Ahlbrandt, M. L. Tuttle, R. R. Charpentier, M. E. Brownfield, K. I.
556 Takahashi, Maps showing geology, oil and gas fields and geological provinces of Africa,
557 *Tech. rep.*, Reston, VA (1997).

558 92. R. M. Pollastro, A. S. Karshbaum, R. J. Viger, Maps showing geology, oil and gas fields
559 and geologic provinces of the Arabian Peninsula, *Tech. rep.*, Reston, VA (1999).

560 93. F. Persits, G. Ulmishek, Maps showing geology, oil and gas fields, and geologic provinces
561 of the Arctic, *Tech. rep.*, Reston, VA (2003).

562 94. D. W. Steinshouer, J. Qiang, P. J. McCabe, R. T. Ryder, Maps showing geology, oil and gas
563 fields, and geologic provinces of the Asia Pacific region, *Tech. rep.*, Reston, VA (1999).

564 95. M. J. Pawlewicz, D. W. Steinshouer, D. L. Gautier, Map showing geology, oil and gas
565 fields, and geologic provinces of Europe including Turkey, *Tech. rep.*, Reston, VA (2002).

566 96. R. M. Pollastro, F. M. Persits, D. W. Steinshouer, Maps showing geology, oil and gas
567 fields, and geologic provinces of Iran, *Tech. rep.*, Reston, VA (1997).

568 97. C. P. Garrity, D. Soller, Database of the geologic map of North America— Adapted from
569 the map by J.C. Reed, Jr. and others (2005), *Tech. rep.*, Reston, VA (2009).

570 98. C. J. Schenk, R. J. Viger, C. P. Anderson, Maps showing geology, oil and gas fields and
571 geologic provinces of the South America region, *Tech. rep.*, Reston, VA (1999).

572 99. F. M. Persits, G. F. Ulmishek, D. W. Steinshouer, Maps showing geology, oil and gas fields
573 and geologic provinces of the former Soviet Union, *Tech. rep.*, Reston, VA (1997).

574 100. A. S. Merdith, S. E. Williams, A. S. Collins, M. G. Tetley, J. A. Mulder, M. L. Blades,
575 A. Young, S. E. Armistead, J. Cannon, S. Zahirovic, *et al.*, Extending full-plate tectonic
576 models into deep time: Linking the Neoproterozoic and the Phanerozoic. *Earth-Science*
577 *Reviews* **214**, 103477 (2021).

578 101. R. D. Müller, J. Cannon, X. Qin, R. J. Watson, M. Gurnis, S. Williams, T. Pfaffelmoser,
579 M. Seton, S. H. Russell, S. Zahirovic, GPlates: building a virtual Earth through deep time.
580 *Geochemistry, Geophysics, Geosystems* **19**, 2243–2261 (2018).

581 102. Z. X. Li, S. V. Bogdanova, A. S. Collins, A. Davidson, B. De Waele, R. E. Ernst, I. C. W.
582 Fitzsimons, R. A. Fuck, D. P. Gladkochub, J. Jacobs, K. E. Karlstrom, S. Lu, L. M. Nat-
583 apov, V. Pease, S. A. Pisarevsky, K. Thrane, V. Vernikovsky, Assembly, configuration, and
584 break-up history of Rodinia: A synthesis. *Precambrian Research* **160**, 179–210 (2008).

585 103. A. Eyster, B. P. Weiss, K. Karlstrom, F. A. Macdonald, Paleomagnetism of the Chuar
586 Group and evaluation of the late Tonian Laurentian apparent polar wander path with im-
587 plications for the makeup and breakup of Rodinia. *Geological Society of America Bulletin*
588 **132**, 710–738 (2020).

589 104. D. A. Evans, The palaeomagnetically viable, long-lived and all-inclusive Rodinia super-
590 continent reconstruction. *Geological Society, London, Special Publications* **327**, 371–404
591 (2009).

592 105. A. B. Ronov, V. Y. Khain, K. Seslavinsky, Vendian lithologic complexes of the world. *Sov.*
593 *Geol.* **5**, 37–59 (1981).

594 106. A. B. Ronov, V. Y. Khain, K. B. Seslavinskiy, Lower and middle riphean lithologic com-
595 plexes of the world. *International Geology Review* **24**, 509–525 (1982).

596 107. D. C. Segessenman, S. Peters, Macrostratigraphy of the Ediacaran System in North Amer-
597 ica. *Preprint at https://doi.org/10.31223/X5Z04M* (2022).

598 108. C. B. Keller, B. Schoene, Statistical geochemistry reveals disruption in secular litho-
599 spheric evolution about 2.5 Gyr ago. *Nature* **485** (2012).

600 109. A. J. Fraass, D. C. Kelly, S. E. Peters, Macroevolutionary History of the Planktic
601 Foraminifera. *Annual Review of Earth and Planetary Sciences* **43**, 139–66 (2015).

602 110. A. D. Rooney, F. A. Macdonald, J. V. Strauss, F. Ö. Dudás, C. Hallmann, D. Selby, Re-
603 Os geochronology and coupled Os-Sr isotope constraints on the Sturtian Snowball Earth.
604 *Proceedings of the National Academy of Sciences* **111**, 51–56 (2014).

605 111. T. M. Gibson, S. Wörndle, P. W. Crockford, T. H. Bui, R. A. Creaser, G. P. Halverson,
606 Radiogenic isotope chemostratigraphy reveals marine and nonmarine depositional envi-
607 ronments in the late Mesoproterozoic Borden Basin, Arctic Canada. *GSA Bulletin* **131**,
608 1965–1978 (2019).

609 112. R. Rainbird, A. Rooney, R. Creaser, T. Skulski, Shale and pyrite Re-Os ages from the
610 Hornby Bay and Amundsen basins provide new chronological markers for Mesoprotero-
611 zoic stratigraphic successions of northern Canada. *Earth and Planetary Science Letters*
612 **548**, 116492 (2020).

113. W. Farrell, J. A. Clark, On postglacial sea level. *Geophysical Journal International* **46**, 647–667 (1976).

114. R. A. Kendall, J. X. Mitrovica, G. A. Milne, On post-glacial sea level–II. Numerical formulation and comparative results on spherically symmetric models. *Geophysical Journal International* **161**, 679–706 (2005).

115. G. A. Milne, J. X. Mitrovica, Postglacial sea-level change on a rotating Earth: first results from a gravitationally self-consistent sea-level equation. *Geophysical Journal International* **126**, F13–F20 (1996).

116. J. X. Mitrovica, J. Wahr, I. Matsuyama, A. Paulson, The rotational stability of an ice-age earth. *Geophysical Journal International* **161**, 491–506 (2005).

117. P. Johnston, The effect of spatially non-uniform water loads on prediction of sea-level change. *Geophysical Journal International* **114**, 615–634 (1993).

118. G. A. Milne, J. X. Mitrovica, J. L. Davis, Near-field hydro-isostasy: the implementation of a revised sea-level equation. *Geophysical Journal International* **139**, 464–482 (1999).

119. K. Lambeck, A. Purcell, P. Johnston, M. Nakada, Y. Yokoyama, Water-load definition in the glacio-hydro-isostatic sea-level equation. *Quaternary Science Reviews* **22**, 309–318 (2003).

120. T. Pico, J. X. Mitrovica, K. L. Ferrier, J. Braun, Global ice volume during MIS 3 inferred from a sea-level analysis of sedimentary core records in the Yellow River Delta. *Quaternary Science Reviews* **152**, 72–79 (2016).

121. A. Dalca, K. Ferrier, J. Mitrovica, J. Perron, G. Milne, J. Creveling, On postglacial sea level—III. Incorporating sediment redistribution. *Geophysical Journal International* **194**, 45–60 (2013).

Acknowledgements: K.D.B. thanks Maggie Osburn, Clint Cowan, and Andy Knoll for providing comments on early drafts of this work and Jess Adkins for being a sounding board for ideas. Seth Finnegan assisted with the Paleobiology Database-derived calcifier diversity curves in Fig. 1G,H. K.D.B. and J.W. thank Shanan Peters for training and encouragement to utilize the Macrostrat database; **Funding:** K.D.B. acknowledges funding from the Packard Foundation and NASA Exobiology Grant 80NSSC19K0464. M.D.C. was supported by a National Defense Science and Engineering Graduate Fellowship; **Author Contributions:** K.D.B. conceptualized the study and wrote the original draft. K.D.B. and J.W. contributed to data investigation, methodology and data curation. J.W. contributed Macrostrat methodology. N.B. and K.D.B contributed software, formal analysis, and visualization. T.P. contributed sea level loading estimates in Fig. 2 and Supplement. B.K. contributed EarthChem data and methodology in Fig. 1C and Fig. 3D. All authors reviewed and edited the manuscript; **Data and materials availability:** All data are provided in the main text or in the supplementary materials. Data, figures, and code are available at Open Science Framework (link) for reviewers and will be made publicly available on manuscript acceptance.

Supplementary Materials :

Materials and Methods

Figs. S1 - S10

References (81 - 120)

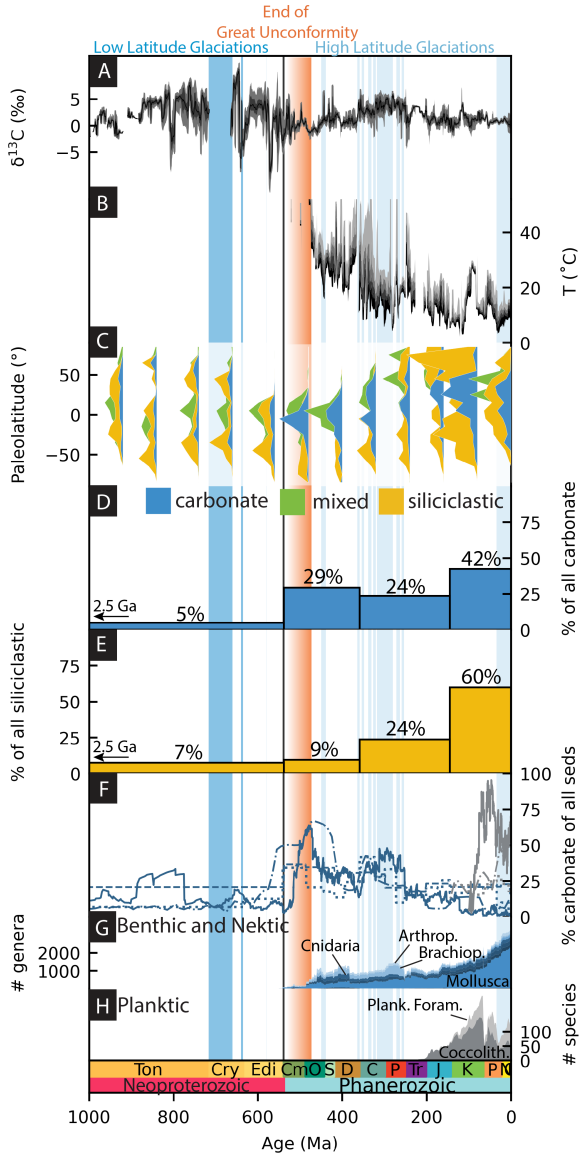

655

656 **Fig. 1. Carbonate isotopic data, the sedimentary record and calcifier biodiversity** (**A**)
657 Quartiles of δ^{13}C from marine carbonates are plotted every 0.5 Myr with a 4 Myr moving
658 window. The second and third quartiles are darkest (*3, 83–86*). (**B**) Quartiles of temperature
659 inferred from fossil δ^{18}O assuming seawater = -1.2‰ (*87*) are plotted every 1 Myr with a 4
660 Myr moving window (*8*). The first quartile is the darkest. (**C**) Histograms estimate probability
661 density functions of Area (m^2) of three sedimentary rock groups by paleolatitude in 80 Myr

bins. The Neoproterozoic probability density function histograms overestimate area because units have poor temporal resolution. Colors are carbonate (blue), mixed (green), and siliciclastic (yellow) (*58*). (**D**) The fraction of carbonate area in each bin to total carbonate area. Bins are 2500–538.8, 538.8–358.9, 358.9–145, 145–0 Ma. (**E**) The fraction of siliciclastic rock area in each bin to total siliciclastic area. Bins are the same as in d. (**F**) The proportion of carbonate to total sediments from our work (continents, dash) (*58, 88*), previous map-based compilations (continents, blue dot, deep sea, grey dot) (*71*), named lithologies among EarthChem sedimentary whole-rock samples (continents, blue dash dot, deep sea, grey dash dot) (*89*), and Macrostrat(continents, blue solid, deep sea, grey solid) (*18, 29*). (**G**) Diversity of benthic and nektic genera that produce calcium carbonate skeletons (*90*). (**H**) Diversity of planktic species of foraminifera and coccolithophores (*18, 19*). Vertical bars indicate events: two Snowball Earth glaciations (dark blue), high latitude glaciations (light blue), the end of the Great Unconformity (orange gradient), the Neoproterozoic–Phanerozoic boundary (bold black line)

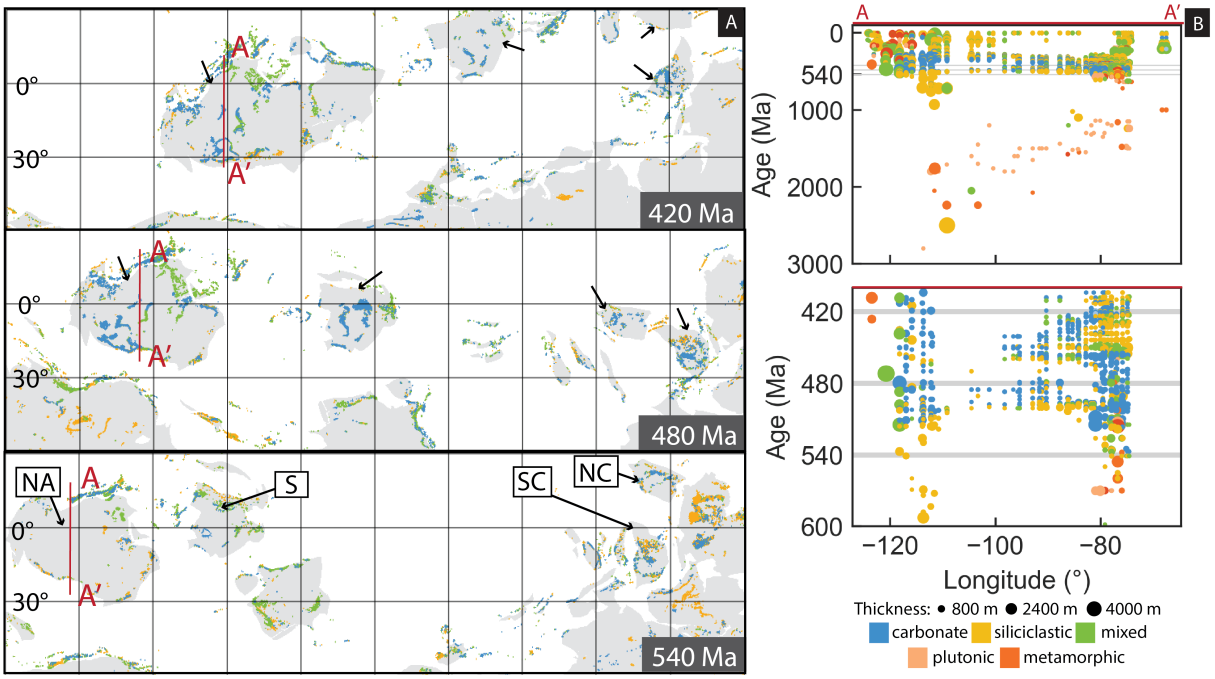

Fig. 2. Spatial distribution of sedimentary rocks and sea-level change caused by carbonate loading at the end of the Great Unconformity (**A**) Time slices at 540, 480 and 420 Ma of surface sedimentary units (*58*). Equatorial land masses include North America (NA), Siberia (S), North China (NC), South China (SC). (**B**) Cross section of the North American continent at present-day 40°N (A-A') showing both thickness and age of each unit using data from (*29*). The lower panel zooms into the 600–400 Ma time window. The cross section of A-A' (red) is shown in (A). The three time slices from (A) are horizontal grey lines.

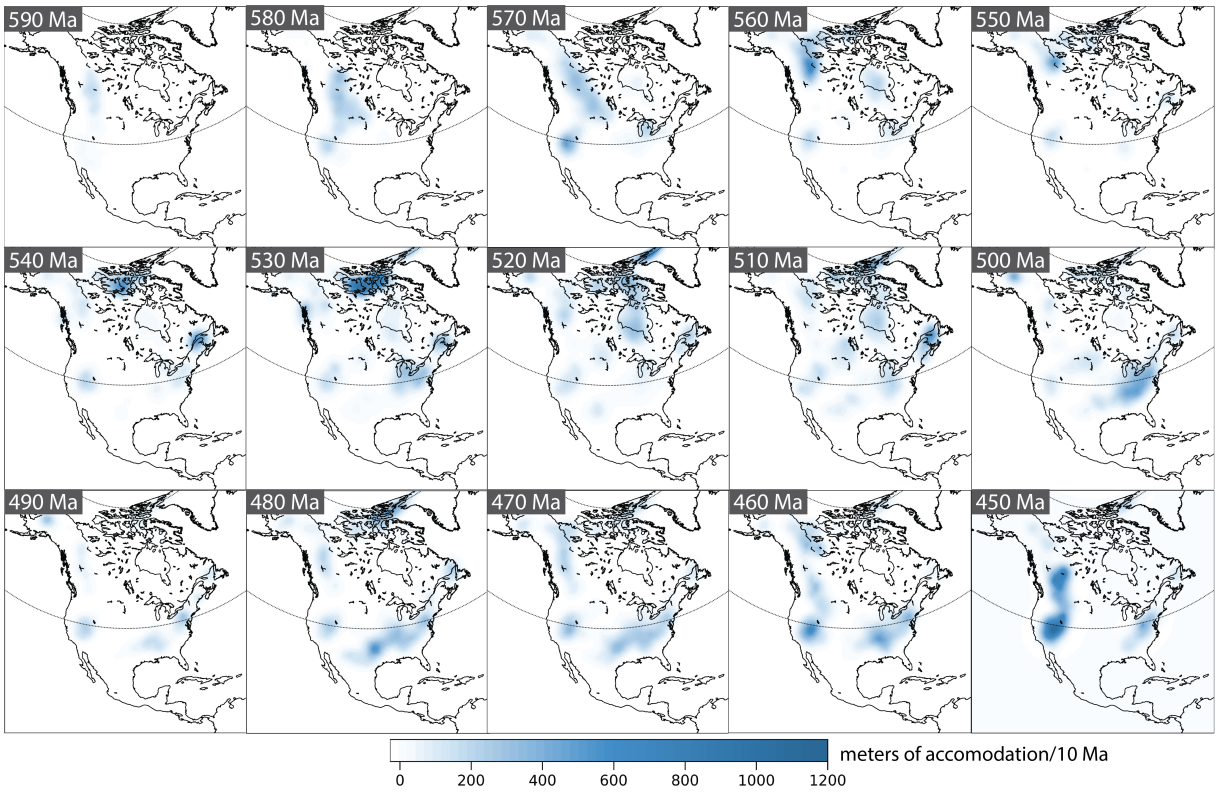

683

684 **Fig. 3. Model of carbonate induced accommodation per 10 million year interval.** Unit
685 thicknesses are partitioned into carbonate and siliciclastic components based on the unit litho-
686 logic description. Carbonate density = 2710 kg/m^3. Rock thickness, age, and lithology data
687 used to calculate sediment loading are from Macrostrat (*29*).

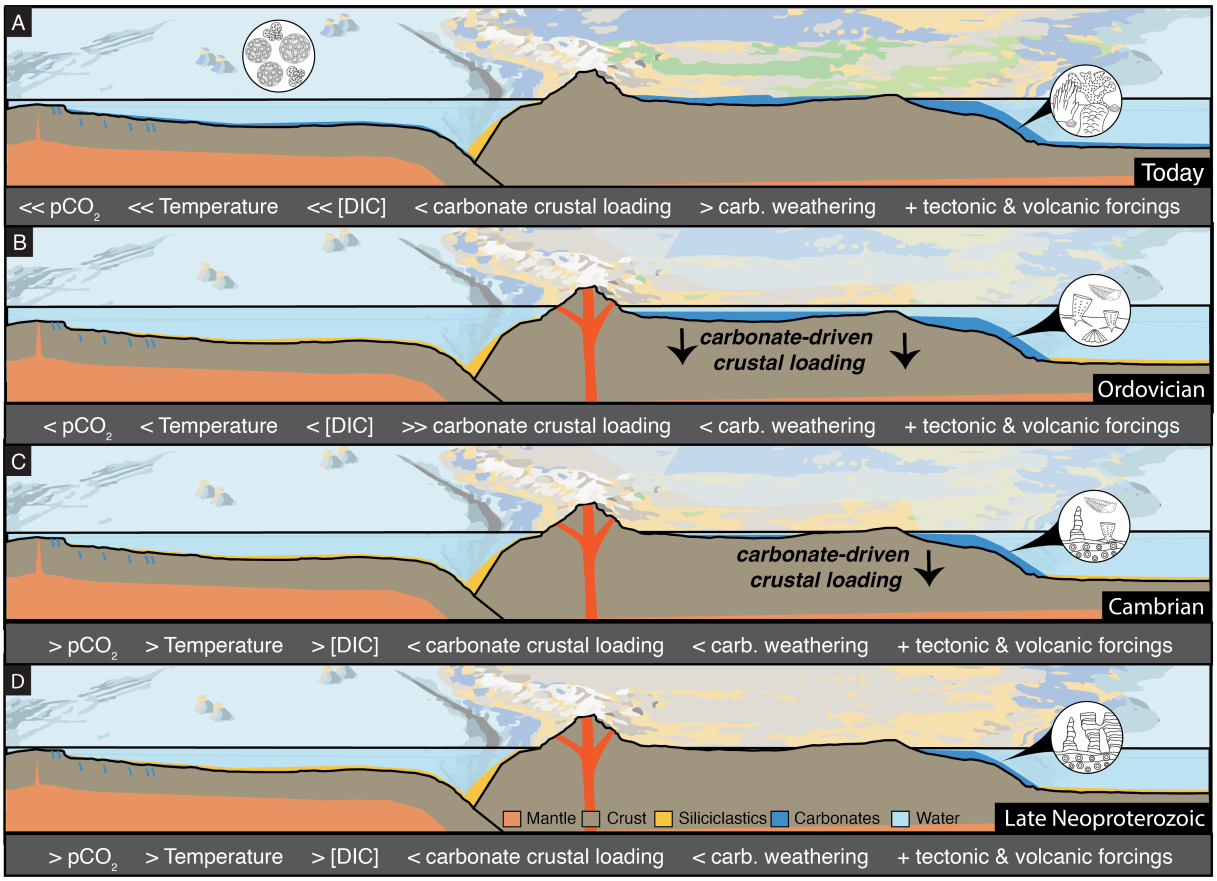

Fig. 4. Conceptual model of proposed changes in carbonate rock reservoir and Earth System impacts through time (**A**) Today diverse carbonate reef builders and calcifying plankton effectively sequester CO_2 on continental margins and the deep sea and efficiently reintroduce carbonate to the mantle. Some continent interiors maintain large carbonate reservoirs formed during the early Paleozoic. (**B**) Ordovician carbonate platform of biomineral-built reefs drives impressive continent-scale progradation of the carbonate platforms and subsidence, effectively sequestering CO_2. (**C**) Cambrian carbonate platform of mixed microbial, abioitic and biomineral-built reefs drives continent-scale progradation of the carbonate platforms and subsidence, effectively sequestering CO_2. (**D**) Late Neoproterozoic carbonate factory is dominated by microbial and abiotic carbonates with small platforms on continental margins.

Supplementary Materials for: Onset of carbonate biomineralization drove global reorganization of sedimentation and subsidence patterns

Authors:

Kristin D. Bergmann, Julia Wilcots, Tamora Pico, Nicholas Boekelheide, Noah T. Anderson, Marjorie D. Cantine,

Samuel L. Goldberg,

Brenhin Keller, Adam B. Jost Athena Eyster

1 Materials and Methods

Global and Regional Lithologic Estimates To estimate potential changes in the size and distribution of the carbonate rock reservoir in the Neoproterozoic and Phanerozoic, we first merged a recent global lithologic map (*88*) with continent-scale and regional geologic maps containing age information from the USGS. The global lithologic map contains about 1.2 million polygons. The map is about 100 times more detailed than previous global lithological maps (*88*). This map is paired with USGS maps from Africa (*91*), Arabia (*92*), Arctic (*93*), Asia (*94*), Europe (*95*), Iran (*96*), North America (*97*), South America (*98*), and Russia (*99*). We assigned a top and bottom age to each lithologic polygon using the ages of the intersecting polygons from the USGS maps. We note that most continent-scale and regional geologic maps do not have good temporal resolution of Proterozoic units (i.e. tags are 'Proterozoic' or at best 'Neoproterozioc') and this represents a source of uncertainty. We recalculated the area of all polygons for a consistent time-dependent lithologic area estimates. We then used a 1000 Ma–present day plate reconstruction underpinned by paleomagnetic data (*100*) in Gplates (*101*) to calculate paleolatitude for the centroid of each of our new age-constrained lithology polygons every 20 Myr. We reimported these polygons into ArcGIS to calculate area through time based on age range and paleolatitude. Data is binned into 80 Myr bins and plotted as histograms (Fig. 1C).

To estimate potential changes in continental carbonates since the start of the Neoproterozoic (1000 Ma), we assessed the area, volume, and proportion of three sedimentary rock groups through time and space: siliciclastic, carbonate, and mixed sediments (both siliciclastics and carbonates)(Fig. 1,2). The definitions of our three sedimentary rock groups are defined by the global lithologic map (*88*)(Fig. 1C,D, Figs. S1,S3,S4,S5). We summed the area of all carbonate polygons within four time bins and compared that area to the total area of all carbonate polygons in our age-delineated global lithologic map dataset (Fig. 1D). We used the same approach with siliciclastic polygons (Fig. 1E).

Despite uncertainties in Neoproterozoic–Ediacaran reconstructions and continental connections ((*50, 102–104*)), the paleogeographies especially important for this work (580 Ma–present) have greater paleomagnetic support and display agreement in paleolatitudes. While the sedimentary unit area by paleolatitude probability density functions may shift as both global reconstructions and age ranges of Precambrian geologic units are improved, the important features uncovered here, namely the early Phanerozoic increase in low latitude carbonates will remain unchanged with choice of paleogeographic reconstruction.

We also compared estimates of the proportion of carbonate to all sedimentary rocks from four datasets relevant to the continental rock reservoir (Fig. 1F). The four include: 1) the proportion of areal extent of carbonates versus total area of sedimentary rocks using our age-delineation of the global lithologic map dataset from (*88*)(Fig. 1F, blue dashed line), 2) a global dataset of area and volume estimated using global lithologic maps created by (*32, 33, 105, 106*)(Fig. 1F, blue dotted line), 3) a North America-specific database that includes subsurface as well as surface geology, estimated maximum and minimum thickness, proportional lithologic information, and areal extent of each unit (Macrostrat, Project ID 1, (*29*))(Fig. 1F, blue solid line). The Ediacaran units have recently been updated (*29, 107*), and 4) named lithologies of continental sedimentary whole-rock sample analyses from the large geochemical EarthChem

database (*89*), plotted using weighted bootstrap resampling approach (*108*)(Fig. 1F, blue dot dash line). For comparison, we also calculated the proportion of deep-sea carbonates to all deep-sea sediments since the Jurassic using three available compilations. The three include: 1) an estimate using drilled ocean sediment cores (*33, 71*)(Fig. 1F, grey dotted line), 2) a second estimate using the thickness and estimated areal extent of many more deep sea sediment cores (Macrostrat Project ID 4) (*109*)(Fig. 1F, grey solid line), 3) and named lithologies of deep-sea sedimentary whole-rock samples from the large geochemical EarthChem database (*89*), plotted using a weighted bootstrap resampling approach (*108*)(Fig. 1F, grey dot dash line).

We assessed regional lithologic patterns across North America using the higher resolution surface and subsurface dataset from Macrostrat (Fig. 2B, Fig. S7) (*29*). To create a 'mixed' group, we created a new category where the siliciclastic and carbonate proportions of a unit were each between 45–55%. The Ediacaran units have recently been updated (*29, 107*). To better reflect the current state of understanding about Mesoproterozoic and Tonian stratigraphy, we also adjusted key thickness and depositional age range estimates in the Macrostrat North America dataset (*29*). We changed the Little Dal Group thickness from 8000 m to 2500 m in the Mackenzie Mountains and the Ashburn Formation thickness from 3500 m to 1500 m. We changed the age range for the Katherine Group to 930–900 Ma and the Little Dal Group to 900–775 Ma across all polygons for consistency (*110*). We updated the depostional age range of the Victor Bay and Arctic Bay formations of the Uluksan Group to 1100–1050 Ma (*111*). We updated the age range of the Angmaat-Nanisivik Formations (formerly Society Cliffs) of the Uluksan Group to 1270–1100 Ma (*111*). In the Shaler Group, we updated the age range of the Glenelg Formation to 1151–1000 Ma, the Reynolds Point Formation to 1000–850, and the Wynniatt Formation to 850–795 Ma (*112*). For our modified Macrostrat Project 1 spreadsheet see (OSFrepository).

Accommodation Calculation To calculate the consequence of sediment load on accommodation, we created a grid using all sedimentary rocks listed as deposited between 600–360 Ma in the North American Macrostrat database (*29*). Grid resolution is 1° latitude and longitude and time resolution is 1 Ma. We opted to partition the thickness of a unit to each lithology (i.e. siliciclastic and carbonate) based on the lithologic description in Macrostrat (*29*) (Fig. 2, Figs. S8,S9,S10,S11).

To calculate the increase in accommodation (ΔSL) in response to carbonate loading, we used a gravitationally self-consistent glacial isostatic adjustment model to solve the sea-level equation (*113*). We perform calculations based on the theory and pseudo-spectral algorithm described by Kendall et al. (2005) with a spherical harmonic truncation at degree and order 512 (*114*). These calculations include the impact of load-induced Earth rotation changes on relative sea-level (*115, 116*), evolving shorelines (*114, 117–119*), and they incorporate a gravitationally self-consistent treatment of sediment loads (*120, 121*). We adopt a one-dimensional Maxwell viscoelastic Earth model VM2, which is characterized by an elastic lithospheric thickness of 120 km, and an average viscosity of 0.3×10^{21} Pa·s and 3×10^{21} Pa·s, for the upper and lower mantle, respectively.

On the multi-million-year timescale relevant for constraining changes in carbonate thickness, we can approximate the solid Earth's response to loading changes as in isostatic equilibrium. Therefore, we adopt the fluid Love numbers associated with the VM2 earth model in our accommodation calculations. In our modeling, we use a density of 2750 kg/m3 for carbonate rocks and 2200 kg/m3 for siliciclastic rocks. We predict the accommodation change due to sediment loading every 10 My from 600–360 Ma (Fig. 3, Figs. S10,S11).

We use estimates for modern North American lithosphere thickness and mantle rheology for our model, despite that Earth structure has changed considerably between the early Paleozoic and today, including crustal thickening on the margins from subsequent mountain-building

events. Such an assumption is required given the challenges associated with reconstructing mantle dynamics in deep time (*59*). Although our predictions will vary with different selected Earth rheology parameters, our results offer a robust first-order assessment of sediment loading across 600-360 Ma.

2 Supplementary information

Fig. S1 To fully explore the global patterns in each continental sedimentary rock reservoir, we considered the total area of each reservoir through time (Fig. S1A), the time normalized total area (Fig. S1B), the proportion of each reservoir to the total sedimentary reservoir through time (Fig. S1C) using our age-delineation of the global lithologic map dataset from (*88*). To explore the contribution of different time periods to each of the continental carbonate and siliciclastic rock reservoirs, we binned the carbonate area relative to the total continental carbonate area and the siliciclastic area relative to the total siliciclastic area (Fig. S1D). Lighter blue and yellow bin–358.9, 358.9–145 , 145–0 Ma] and darker blue and yellow bins are [1000–538.8, 538.8–486.9, 486.9–443.1, 443.1–419, 419–359.3, 359.3–323.4, 323.4–307, 307–298.9, 298.9–251.9, 251.9–201.4, 201.4–143.1, 143.1–66, 66–56, 56–33.9, 33.9–23.04, 23.04–5.33, 5.33–2.58, 2.58–0.0117, 0.0117–0 Ma] respectively. To explore the importance of the mixed group we added 20% of the mixed area to the carbonate bins (lightest blue) and 80% of the mixed area to the siliciclastic bins (lightest yellow). This does not significantly alter the relative contribution of any bin. The proportion of carbonates and siliciclastics to total area of each reservoir in the four longer time bins do not follow the same pattern. Proterozoic rocks are a minor contribution to the total carbonate reservoir (5%) especially when compared to the large early Phanerozoic carbonate contribution (29%, Fig. 1D). In contrast, the siliciclastics within these time intervals represent a minor proportion of all siliciclastic rocks (Proterozoic: 7% and Early Phanerozoic: 9%), Fig. 1E). Indeed, younger siliciclastic rocks are an

increasingly large portion of their total reservoir whereas the fraction of carbonate is more stable across the Phanerozoic. Mixed depositional systems show a modest increase in area across the Neoproterozoic–Phanerozoic boundary. Taking their contribution into account in each time bin, the time-varying proportions of carbonates and siliciclastics barely change (Fig. 1C), Fig. S1). Most continent-scale geologic maps do not have good temporal resolution of Proterozoic units (i.e., tags are "Proterozoic" or "Neoproterozoic") and this represents a source of uncertainty. We chose to bin the entire Proterozoic in Fig. 1C,D for this reason, which makes the differences between carbonate and siliciclastic rock in the Proterozoic and Early Phanerozoic bins even more surprising.

Fig. S2 We calculate rough estimates of CO_2 sequestration in GtC/yr into the continental and deep sea carbonate rock reservoirs through time based on the current, preserved sedimentary rock record (Fig. S2A). To calculate volume from our age-delineated, global lithologic map dataset from (*88*), we assumed a constant carbonate thickness of 178 m over the entire time interval and all regions (Fig. S2, blue dashed lines). This represents the average maximum thickness of carbonate units in North America from Macrostrat (*29*). We compare this estimate of the flux of GtC/yr to one using the Macrostrat North America and deep sea projects (projects = 1 and 4) (*29, 109*)(Fig. S2, blue and grey solid lines). For the deep sea database we only calculate volume using the thickness data in combination with the area of the Atlantic Ocean as that is where most of the cores in Project ID 4 are from (*109*). Without a better resolved global ocean time series, this is only a rough estimate of the GtC/yr sequestered in the deep sea carbonate reservoir. We also include an estimate of GtC/yr sequestered into the two carbonate rock reservoirs from global dataset of area and volume estimated using global lithologic maps created by (*32, 105, 106*)(Fig. S2, blue dotted line)and the deep sea using drilled ocean sediment cores (*33, 71*)(Fig. S2, grey dotted line) (Fig. S2). We use the burial flux from the

existing map based area (*88*) and the Macrostrat-based deep sea burial flux estimate (*29, 109*) to estimate residence time of inorganic carbon in the ocean using the modern size of the DIC reservoir over the entire time interval (38973 GtC) and with a larger reservoir in the Precambrian and early Paleozoic that was ultimately sequestered in early Paleozoic carbonates (101000 GtC). Residence time increases to 1-2.5 million years in the Precambrian if one assumes shallow nearshore environments are the dominant carbonate sequestering environment before the evolution of planktonic calcifiying organisms (Fig. S2B).

Figs. S3,S4 We explore changes in area and proportion of each lithology at the regional-scale and note the locations with significant increases in sedimentary rocks across the Proterozoic–Phanerozoic transition are dominated by carbonate (Figs. S3,S4).

Figs. S5,S6, Movie S1 To explore the data at the most granular map scale through time we use ArcGIS to replot the lithologic polygons from our age-delineation of the global lithologic map dataset from (*88*) with centroid paleolatitude constraints from the plate reconstruction by (*100*) in Gplates (*101*) every 10 Myr. For comparison, we also include different geologic maps of North America, Siberia, and China from Macrostrat denoting Ediacaran rocks (pink) and Cambrian–Ordovician rocks (greens)(Fig. S6) (*29*). If anything this comparison suggests the global lithologic map from (*88*) might underestimate the area of Cambrian–Ordovician sedimentary rocks in North America, Siberia and China.

Fig. S7 To visualize the dynamics of carbonate sedimentation across North America in more detail, we create cross sections of the North American continent at present-day 40°N (Fig. 2c), 35°N, 65°N, 90°W, 120°W (Fig. S7) showing both thickness and age of each unit (i.e., a Wheeler Diagram) using data from (*29*). We partitioned the units in siliciclastic and carbonate thicknesses using Macrostrat lithologic descriptions (Figs. 2C, S7). To create a 'mixed' group,

we created a new category where the siliciclastic and carbonate proportions of a unit were between 45–55%.

Figs. S8, S9, S10 To understand the predicted sea-level contribution from sediment loading by siliciclastic and carbonate lithologies, we first binned the loads into three 60 million year intervals (Fig. S8). To better compare across lithologies, Fig. S8 uses a color bar from 0–2000 m/60 Myr where the most saturated color represents the maximum accommodation from carbonate loading. We explored the more granular contribution to accommodation from each lithology in 10 Myr intervals (Figs. S9,S10).

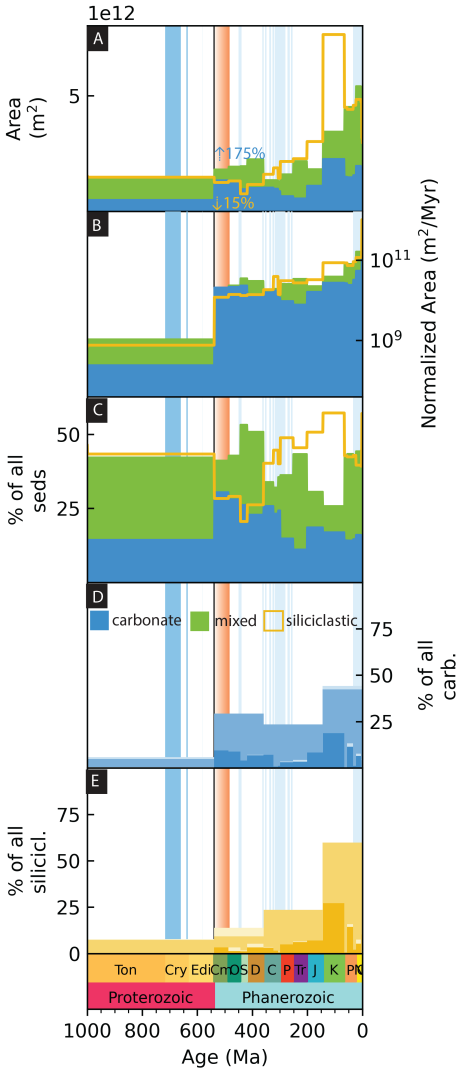

Fig. S1. Total area and proportion of sediments through time. (**A**) Area of exposed sedimentary rocks calculated by combining a global lithologic map (*88*) and continent-scale geologic maps (*91–99*). The Neoproterozoic areas are overestimates because units have poor temporal resolution. (**B**) Area of exposed sedimentary rocks divided by the duration of the time bin (m^2/Myr). (**C**) The proportion of each rock type compared to all sedimentary rocks within a given time bin. (**D**) Percent of carbonate rocks to all carbonate rocks within two sets of time bins (blue) and assuming 20% of mixed sedimentary rocks are also carbonate (lighter blue).

(**E**) Percent of siliciclastic rocks to all siliciclastic rocks within two sets of time bins (yellow) and assuming 80% of mixed sedimentary rocks are also siliciclastic (light yellow) (*58*). Vertical bars indicate events: two Snowball Earth glaciations (dark blue), high latitude glaciations (light blue), the end of the Great Unconformity (orange gradient), the Neoproterozoic–Phanerozoic boundary (bold black line).

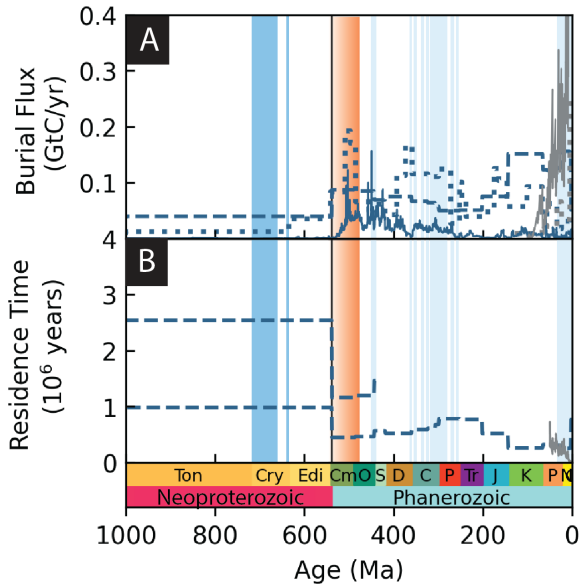

Fig. 5. Inorganic carbon burial flux and residence time (**A**) Estimates of marine inorganic carbon burial flux in GtC/yr (See Methods) using the global lithologic map dataset (continents, dash) (*88*), previous map-based compilations (continents, blue dot, deep sea, grey dot) (*71*), and Macrostrat(continents, blue solid, deep sea, grey solid) (*18, 29*). All estimates support an increase in carbon sequestration in the early Phanerozoic. (**B**) Estimates of residence time in millions of years using the global lithologic map-based burial flux estimate (continents, dash) and two DIC pool sizes, 38973 GtC (modern) and 101000 GtC (Precambrian-Ordovician), and the Macrostrat-based deep sea burial flux estimate, grey solid) (*18, 29*) (*58*). Vertical bars indicate events: two Snowball Earth glaciations (dark blue), high latitude glaciations (light blue), the end of the Great Unconformity (orange gradient), the Neoproterozoic–Phanerozoic boundary (bold black line).

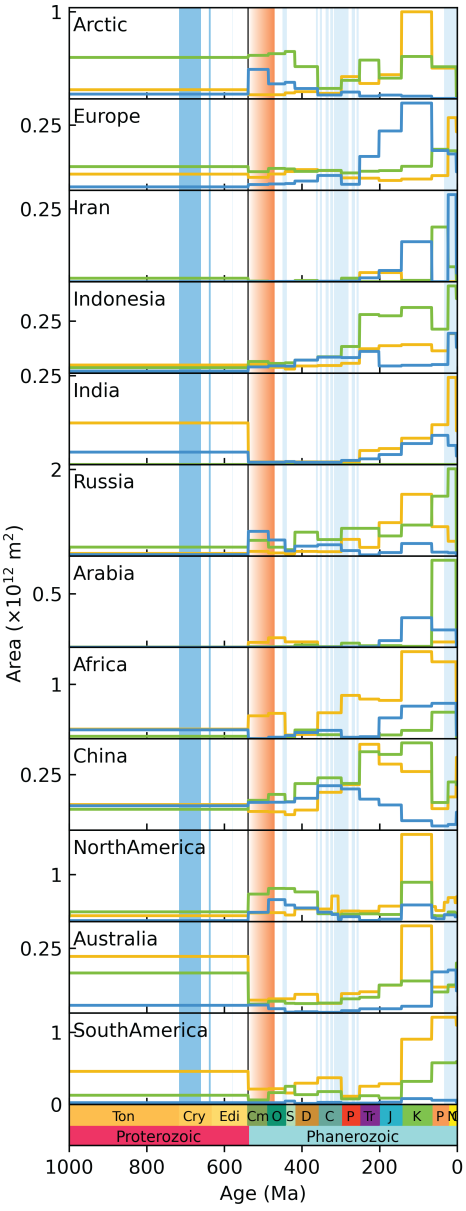

Fig. S3. Total area of sedimentary rock types by region Carbonate (blue), siliciclastic (yellow), mixed carbonate-siliciclastic (green). Vertical light blue boxes indicate periods of glaciation. The bold vertical line indicates the Neoproterozoic–Phanerozoic boundary.

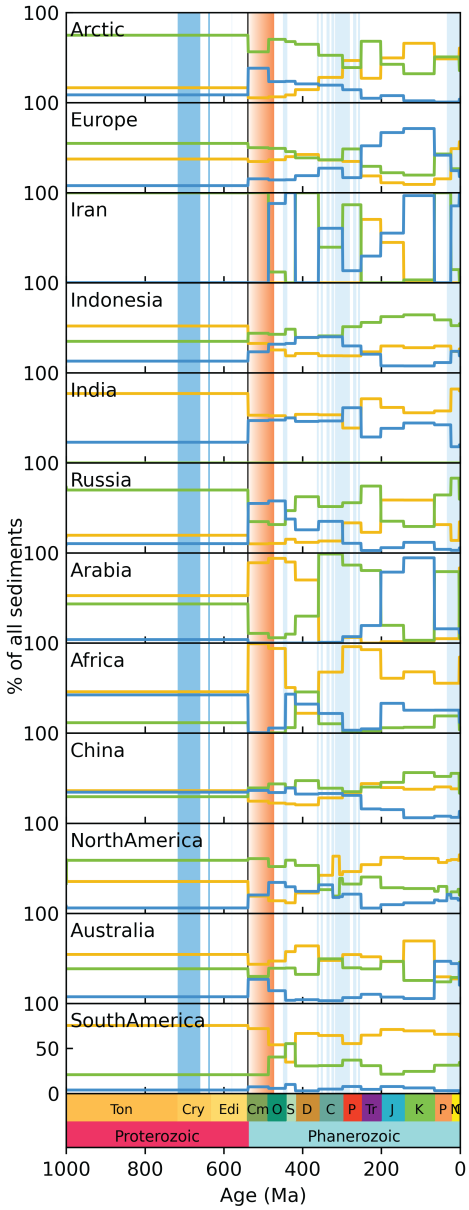

Fig. S4. The proportion of sedimentary rock types by time by region. Carbonate (blue), siliciclastic (yellow), mixed carbonate-siliciclastic (green). Vertical light blue boxes indicate periods of glaciation. The bold vertical line indicates the Neoproterozoic–Phanerozoic boundary.

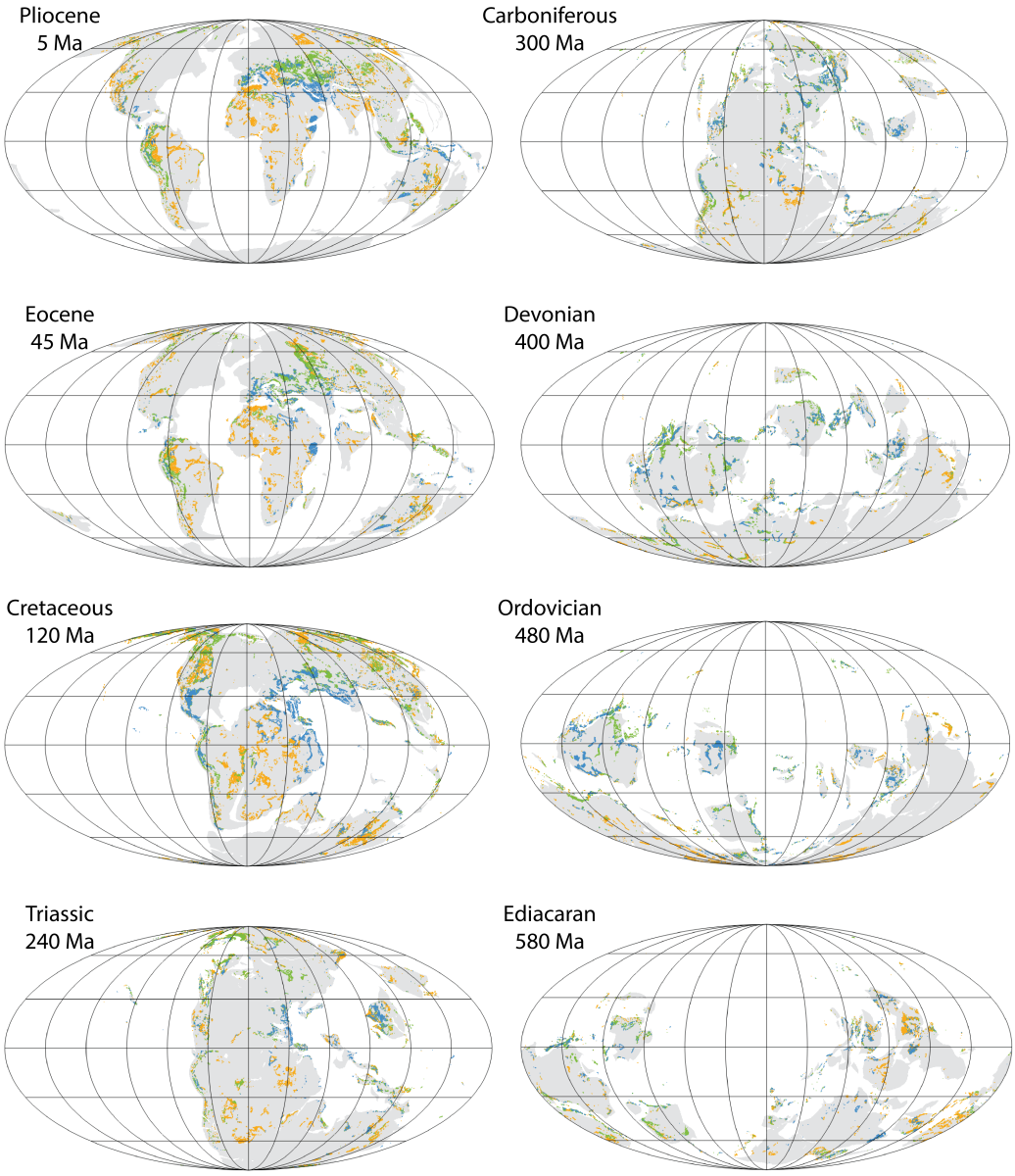

910

911 **Fig. S5. Series of global lithologic maps through time.** Area of exposed sedimentary rocks
912 calculated by combining a global lithologic map (*88*) and continent-scale geologic maps (*91–*
913 *99*). Carbonate: blue, siliciclastic: yellow, mixed carbonate-siliciclastic: green.

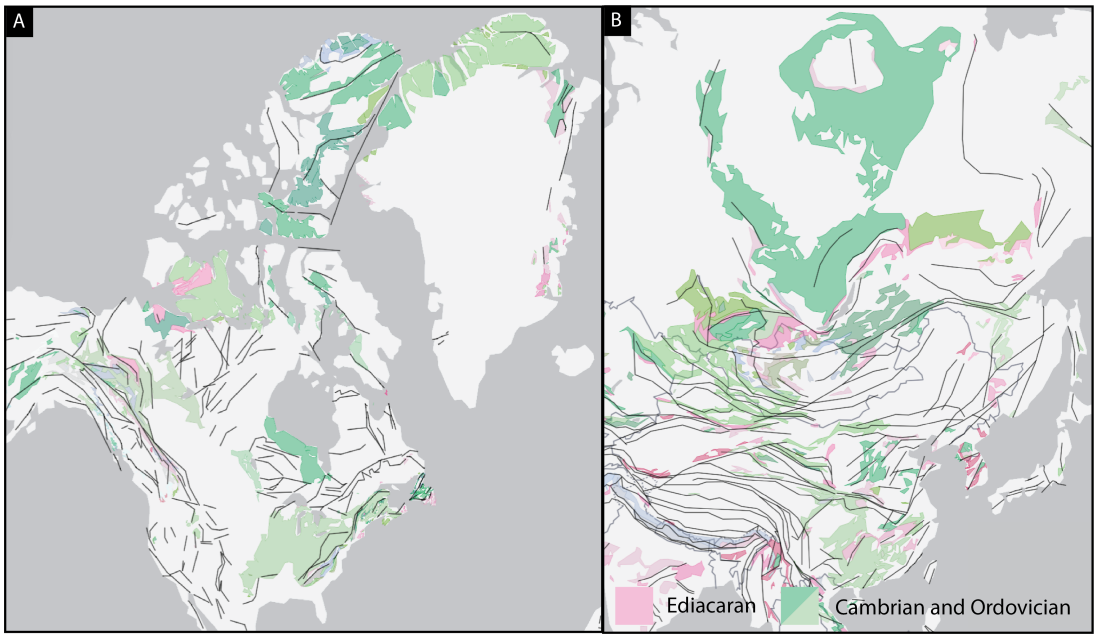

Fig. S6. Map of Ediacaran and Cambrian–Ordovician aged rocks from Macrostrat. (**A**) Map of Ediacaran and Cambrian–Ordovician aged rocks in North America. (**B**) Map of Ediacaran and Cambrian–Ordovician aged rocks in Siberia and Asia. Filtered map from Macrostrat of Ediacaran (pink) rocks and Cambrian–Ordovician rocks (greens) (*29*). Most are sedimentary rocks but not all.

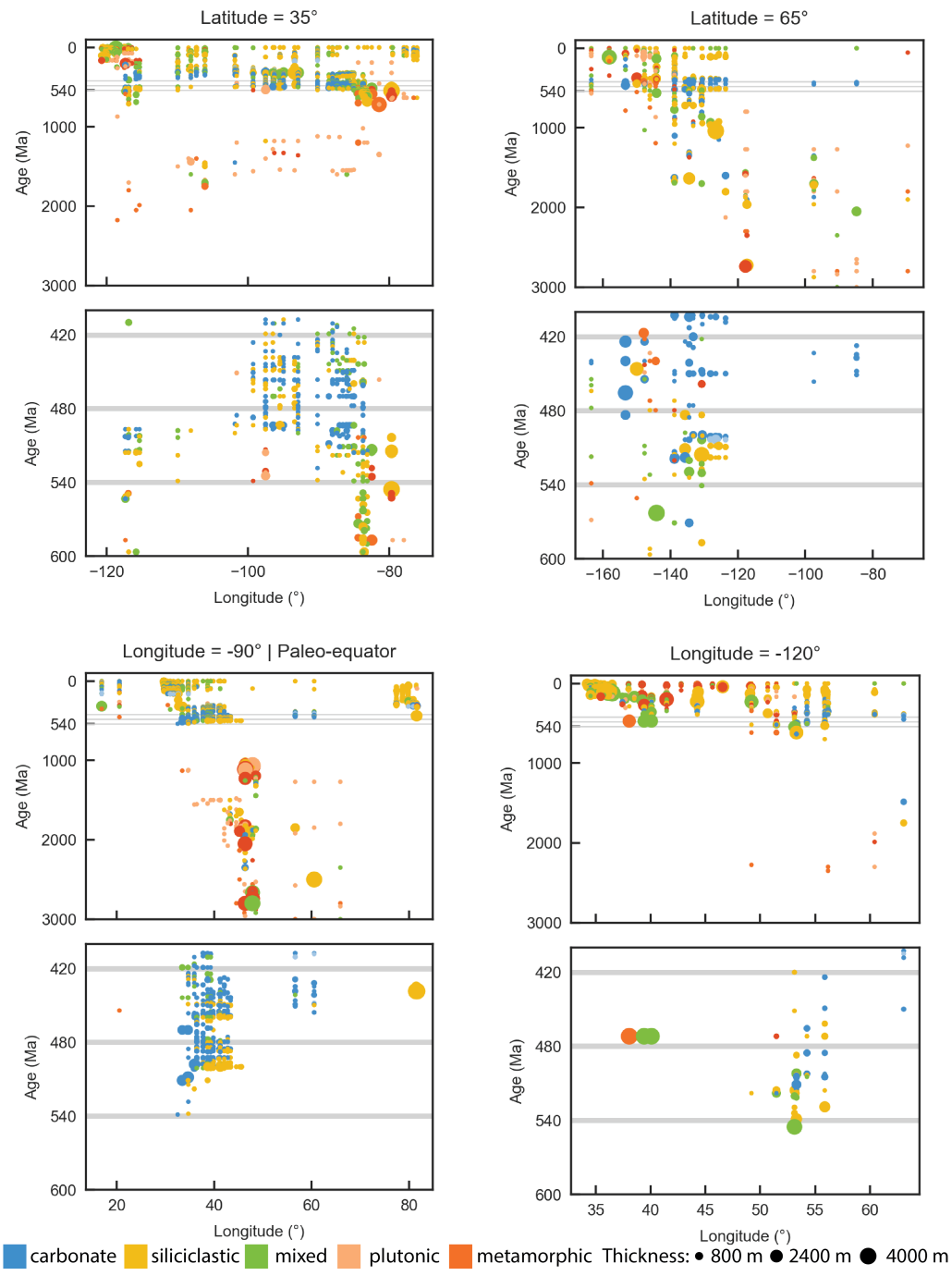

Fig. S7. Cross continent cross sections of North America. Cross sections at present-day 35°N, 65°N, 90°W, and 120°W. The three time slices and 60 million year bin dividers from Fig. 2 are shown as grey lines. Rock thickness, age, and lithology data used to calculate sediment

924 loading are from Macrostrat (*29*). Carbonate: blue, siliciclastic: yellow, mixed carbonate-
925 siliciclastic: green, igneous and metamorphic: pink and red.

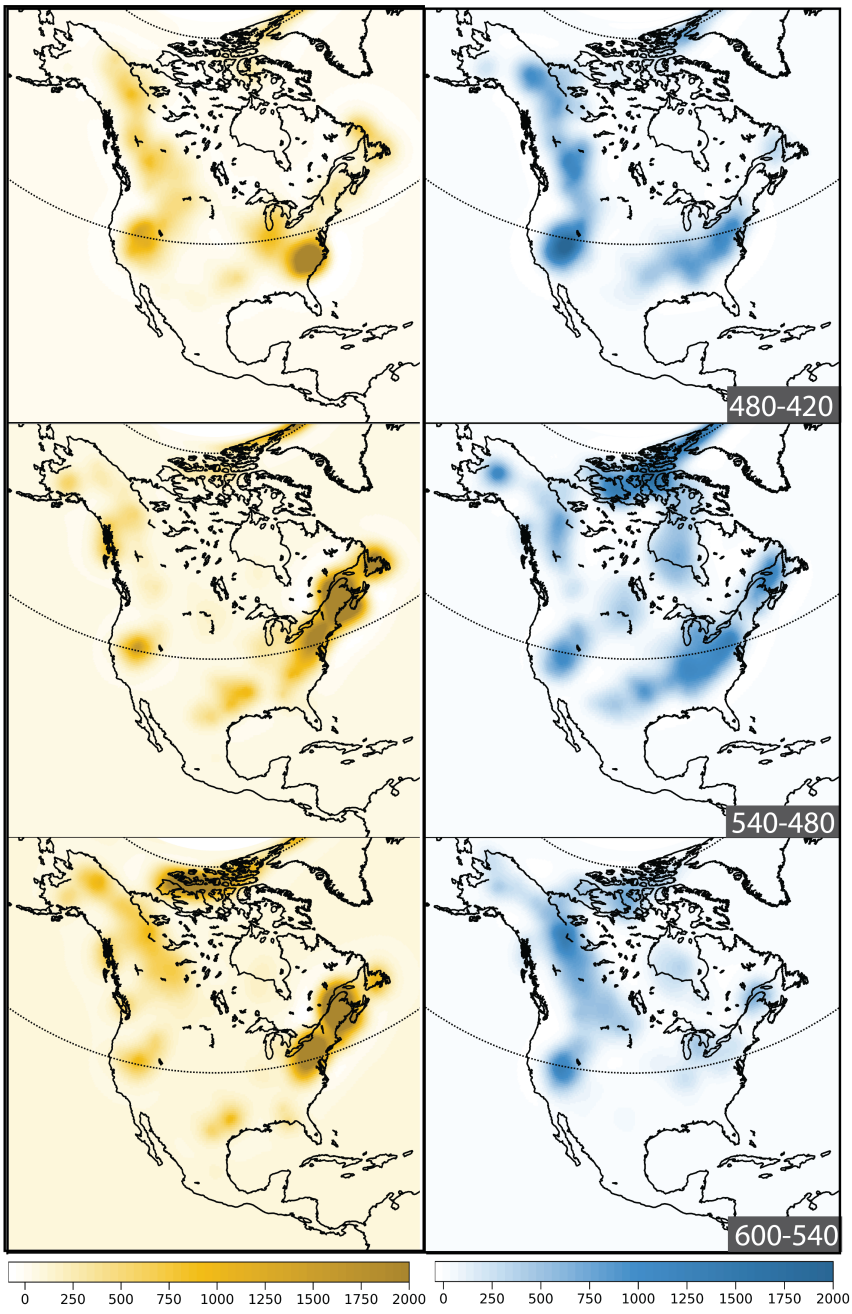

Fig. S8. Model of siliciclastic and carbonate induced accommodation per 60 million year interval. Bins are 600–540, 540–480, 480–420 Ma. Color bars for siliciclastic-driven (yellow) and carbonate-driven (blue) accommodation are saturated for carbonate (2000 m/60 Myr), while siliciclastic rocks can create up to 6000 m/60 Myr of accomodation at their maximum (i.e. the

931 Taconic Orogeny). Unit thicknesses are partitioned into carbonate and siliciclastic thicknesses
932 based on the unit lithologic description. Carbonate density = 2710 kg/m^3, and siliciclastic
933 density = 2200 kg/m^3. Rock thickness, age, and lithology data used to calculate sediment
934 loading are from Macrostrat (*29*).

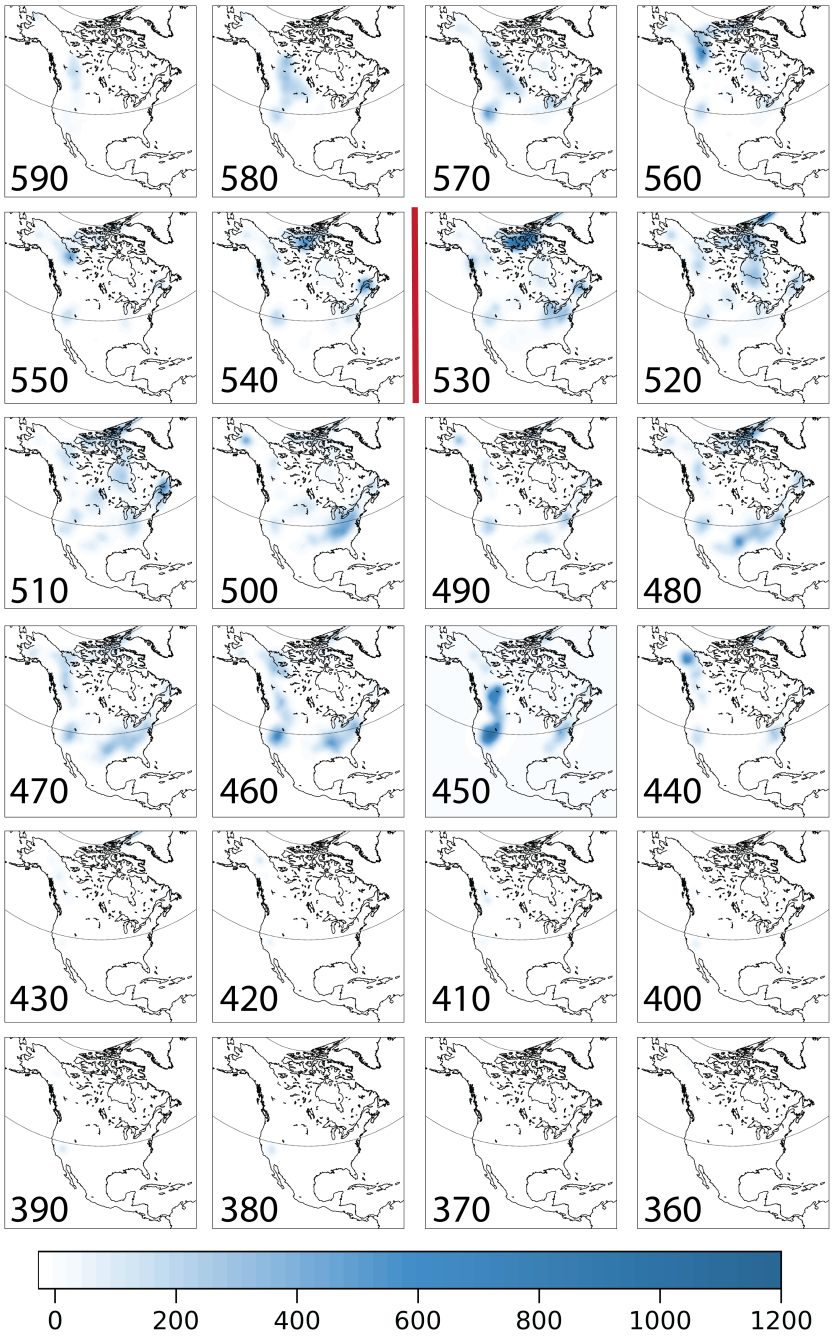

935

936 **Fig. S9. Model of carbonate induced accommodation per 10 million year interval.** Unit
937 thicknesses are partitioned into carbonate and siliciclastic components based on the unit litho-
938 logic description. Carbonate density = 2710 kg/m^3. Red line identifies the interval containing

939 the Neoproterozoic-Phanerozoic boundary. Rock thickness, age, and lithology data used to
940 calculate sediment loading are from Macrostrat (*29*).

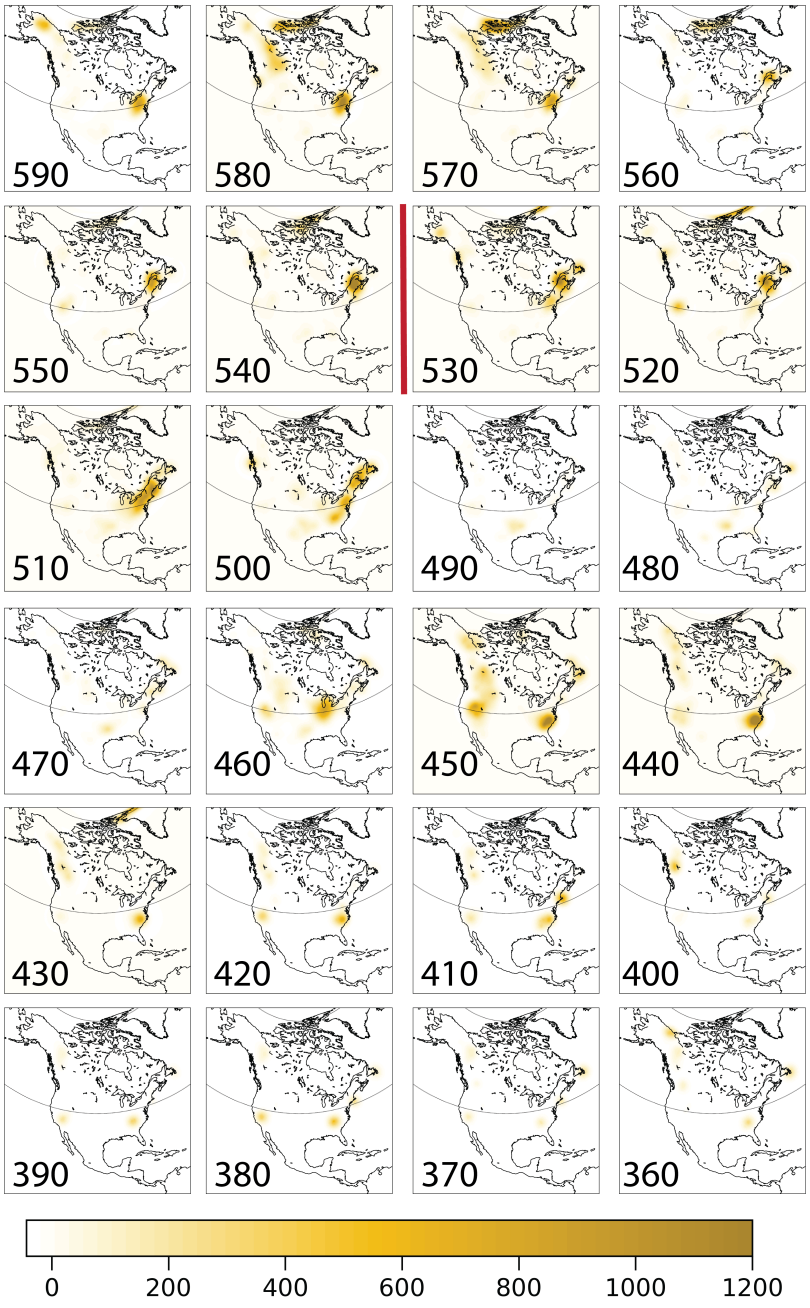

941

942 **Fig. S10. Model of siliciclastic induced accommodation per 10 million year interval.** Unit
943 thicknesses are partitioned into carbonate and siliciclastic components based on the unit litho-
944 logic description. Siliciclastic density = 2200 kg/m^3. Red line identifies the interval containing
945 the Neoproterozoic–Phanerozoic boundary. Rock thickness, age, and lithology data used to

946 calculate sediment loading are from Macrostrat (*29*).